788 J. Med. Chem. 2011, 54, 788–808
DOI: 10.1021/jm101063h

Journal of Medicinal Chemistry Article

Identification of Diaryl Ether-Based Ligands for Estrogen-Related Receptor α as Potential Antidiabetic Agents†

Raymond J. Patch, Lily L. Searle, Alexander J. Kim, Debyendu De, Xizhen Zhu, Hossein B. Askari, John C. O'Neill, Marta C. Abad, Dionisios Rentzeperis, Jianying Liu, Michael Kemmerer, Ling Lin, Jyotsna Kasturi, John G. Geisler, James M. Lenhard, Mark R. Player,* and Micheal D. Gaul

Johnson & Johnson Pharmaceutical Research and Development, Welsh and McKean Roads, Spring House, Pennsylvania 19477-0776, United States

Received August 16, 2010

Estrogen-related receptor α (ERRα) is an orphan nuclear receptor that has been functionally implicated in the regulation of energy homeostasis. Herein is described the development of diaryl ether based thiazolidenediones, which function as selective ligands against this receptor. Series optimization provided several potent analogues that inhibit the recruitment of a coactivator peptide fragment in in vitro biochemical assays (IC_{50} < 150 nM) and cellular two-hybrid reporter assays against the ligand binding domain (IC_{50} = 1−5 μM). A cocrystal structure of the ligand-binding domain of ERRα with lead compound **29** revealed the presence of a covalent interaction between the protein and ligand, which has been shown to be reversible. In diet-induced murine models of obesity and in an overt diabetic rat model, oral administration of **29** normalized insulin and circulating triglyceride levels, improved insulin sensitivity, and was body weight neutral. This provides the first demonstration of functional activities of an ERRα ligand in metabolic animal models.

Introduction

Nuclear receptors (NRs[a]) comprise a group of structurally similar proteins that function as transcription factors that regulate a range of cellular functions including growth, differentiation, and proliferation.[1] In their inactivated states, NRs are typically associated with repressor proteins, which preclude their DNA transcriptional activities.[2] Activation of these receptors, often through ligand binding, induces a conformational change that results in the dissociation of the repressor protein from the NR and subsequent recruitment of coactivator proteins; these resulting complexes bind to response elements within the promoter region of their target genes.[2] For many nuclear receptors, endogenous and/or synthetic ligands have been identified, thereby facilitating the delineation of normal functional roles as well as pathophysiological consequences of aberrant activation of these proteins. However, almost half of the currently recognized NRs are orphan receptors, whose endogenous ligands and precise physiological roles have yet to be identified. The estrogen-related receptors (ERRs) are a subfamily of such nuclear orphan receptors, which were identified on the basis of sequence similarities of their DNA binding domains with those of the estrogen receptors (ER-α and ER-β). However, unlike these ERs, the ERRs do not bind natural estrogen ligands and are in fact constitutively active in the sense that they do not require a ligand-induced conformational change in order to promote coactivator binding.

ERRα and ERRβ were the first estrogen-related receptors to be identified, having been isolated by a low stringency hybridization screen.[3] More recently, a third member of this orphan receptor subfamily, ERRγ, has been identified.[4] The ERRs and ERs share sequence similarities, with the highest homologies (~60%) observed in their DNA-binding domains. While preferentially binding DNA sites termed ERR response elements (ERREs), ERRs additionally interact with the classical DNA estrogen response elements (EREs).[5] Recent biochemical evidence suggests that the ERRs and ERs share target genes, including pS2,[6] lactoferrin,[7] aromatase,[7] and osteopontin[8,9] and additionally share several co-regulatory proteins. Additionally, cross-talk between ERRs and ERs has been described for several of these genes.[10] Thus, the ERRs may provide compensatory functional responses or may directly modulate estrogenic signals in some tissues.[11,12] Since estrogenic effects are primarily mediated in the breast, bone and endometrium, ERR modulators may prove useful in the treatment of bone-related diseases, breast cancer, and gynecological disorders.

Much evidence has also been accumulated supporting a primary role of ERRα in the regulation of metabolism and energy homeostasis. This nuclear receptor is regulated by

†Coordinates of the ERRα crystal structure in complex with **29** have been deposited in the Protein Data Bank (PDB code 3K6P).

*To whom correspondence should be addressed. Phone: 215-628-7860. Fax: 215-540-4616. E-mail: mplayer@its.jnj.com.

[a] Abbreviations: NR, nuclear receptor; ERR, estrogen-related receptor; ER, estrogen receptor; ERE, estrogen response element; ERRE, estrogen-related receptor response element; LBD, ligand binding domain; PPAR, peroxisome proliferator-activated receptor; PGC-1, peroxisome proliferator-activated receptor γ coactivator 1; OXPHOS, oxidative phosphorylation; RIP-140, receptor-interacting protein 140; PEPCK, phosphoenolpyruvate carboxykinase; MCAD, medium-chain acyl coenzyme A dehydrogenase; PDK, pyruvate dehydrogenase kinase; apoA-IV, apolipoprotein A-IV; $ERR\alpha^{-/-}$, ERRα null; FRET, fluorescence resonance energy transfer; TR-FRET, time-resolved fluorescence resonance energy transfer; hSRC, human steroid receptor coactivator; TZD, thiazolidine-2,4-dione; CYP, cytochrome P450; HLM, human liver microsomes; MLM, mouse liver microsomes; RLM, rat liver microsomes; LBD, ligand binding domain; LXR, liver X receptor; RAR, retinoic acid receptor; E2, 3,17β-estradiol; AF-2, activation function 2; TG, triglyceride; FFA, free fatty acids; OGTT, oral glucose-tolerance test; DIO, diet-induced obesity.

 Published on Web 01/10/2011

coactivator and co-repressor proteins with recognized functions in metabolic processes, and it likewise activates the transcription of several gene targets that are involved in metabolic regulation and energy expenditure. ERRα is predominately expressed in tissues that derive energy from lipid metabolism, such as heart, intestine, kidney, skeletal muscle, and adipose tissue. Its expression profile correlates with that of PPARγ coactivator-1 proteins (isoforms PGC-1α and PGC-1β), principal metabolic modulators for several transcription factors that have additionally been shown to function as potent ERRα coactivator ligand proteins.[13−16] In fact, a reciprocal transcriptional capacity between PGC-1α and ERRα has been noted, wherein the two proteins are capable of influencing the transcriptional activities of each other.[17] It has been found that PGC-1α targeted genes involved in oxidative phosphorylation (OXPHOS) are down-regulated in human diabetic skeletal muscle, and evidence suggests that this may be attributed, at least in part, to ERRα function.[18] The energy regulating co-repressor ligand, receptor-interacting protein 140 (RIP-140), which suppresses the expression of several genes involved in glucose and lipid metabolism,[19,20] has also been shown to interact with ERRα and affect its target gene transactivations.[21] In turn, ERRα up-regulates RIP-140 gene transcription during adipogenesis,[22] implicating a role for the former in maintaining energy homeostasis in adipocytes. Additionally, it has been demonstrated that ERRα can repress the transcription of the phosphoenolpyruvate carboxykinase (PEPCK) gene, which encodes a rate-determining gluconeogenic enzyme.[23]

One of the first target genes identified for ERRα and linking this orphan receptor to a possible role in lipid metabolism was *Acadm*, the gene encoding medium-chain acyl coenzyme A dehydrogenase (MCAD), which is a rate-limiting enzyme that catalyzes the initial step of mitochondrial fatty acid β-oxidation. ERRα was shown to regulate the transcription of *Acadm* in vitro[24] by a process that depends on PGC-1 coactivation.[14]

Pyruvate dehydrogenase kinase 4 (PDK4), a key regulatory enzyme whose activity ultimately leads to reduced glucose metabolism, has also been shown to be expressed in response to ERRα/PGC-1α-driven transcription in muscle and hepatocytes.[25−27] Since expression of PDK genes is elevated in diabetic animals,[28] a role for ERRα in the course of this disease may be implicated.

Apolipoprotein A-IV (apoA-IV), a satiety signal that is synthesized in the intestine following lipid ingestion, has also been reported to be basally transcribed by ERRα, and an ERRα regulatory function in intestinal lipid transport and energy homeostasis has been suggested.[29]

While biochemical studies have provided support for a modulatory role of ERRα in metabolic processes, perhaps a better understanding of its functions in vivo has been gleaned from the phenotypic analysis of ERRα-deficient (ERRα$^{-/-}$) mice.[30] The ERRα$^{-/-}$ mouse is viable and notably lean, exhibiting reduced adiposity (∼20%) compared with wild-type controls. Furthermore, this reduction in body fat does not appear to be attributable to altered food consumption. In addition, ERRα$^{-/-}$ null mice are resistant to weight gain under a high-fat diet. Gene expression profiling of adipose tissue from these mice has revealed altered expression of several genes encoding enzymes involved in lipid metabolism, including *Acadm*, which is up-regulated. Lipogenesis is also significantly reduced in these mice, as is an altered expression of intestinal lipid digestion and absorption genes, all of which are consistent with the observed resistance to diet-induced obesity. The latter is especially manifested in the phenotype of ERRα$^{-/-}$ pups, which exhibit significant lipid malabsorption.[29]

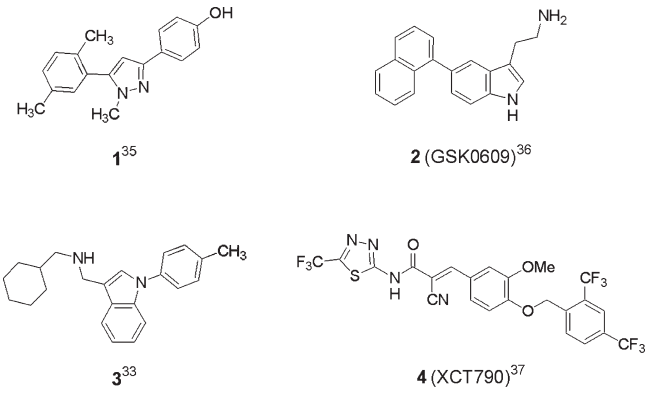

1[35] **2** (GSK0609)[36] **3**[33] **4** (XCT790)[37]

Figure 1. Structures of reported ERRα inverse agonists.

Thus, extensive biochemical and pharmacological studies highlight the complex regulatory functions of ERRα with respect to the maintenance of energy homeostasis and metabolism. Its apparently prominent role in this regard has sparked much interest in this receptor as a potential therapeutic target in the treatment of such metabolic disorders as diabetes and obesity. However, differential expression of cognate coactivator and co-repressor proteins coupled with an extensive network of transcriptional targets gives rise to pleiotropic effects, thus making it difficult a priori to predict the therapeutic outcome of selective ERRα receptor modulation in a disease state. Some have speculated that positive modulators of ERRα receptor activity would have utility in the treatment of metabolic disorders, since such putative agents might be expected to increase the expression of PGC-1α- and PGC-1β-responsive OXPHOS genes that are otherwise down-regulated in diseases such as diabetes.[18,31] Such agents might also be expected to suppress hepatic gluconeogenesis by enhancing repression of PEPCK gene transcription.[23] On the other hand, ERRα inverse agonists could provide antidiabetic effects by normalizing the attenuated glucose utilization levels that would result from inappropriately increased PDK4 expression and activity.

Recent structural studies have provided insight into the differences between active and inactive conformations of ERRα's ligand-binding domain (LBD).[32,33] The observation of a largely occluded ligand binding pocket in the transcriptionally active conformation has led some to the conclusion that ERRα does not lend itself to direct activation by small molecule agents.[34] Consistent with this notion, only a few reports have appeared to date describing selective ligands for ERRα receptor modulation, and these have been limited to inverse agonists (Figure 1). A series of pyrazoles that functionally antagonize the ERRα receptor was disclosed, of which a specified compound (**1**) was claimed to reduce the activity of an ERRα-driven reporter gene in HEK293 cells ($EC_{50} \approx 1-5\ \mu M$).[35] Biarylindole **2** has been reported as a submicromolar inverse agonist of ERRα in a two-hybrid assay and has allowed for structural insight into the mechanism of receptor inhibition.[36] *N*-Arylindole **3** has been reported to bind to ERRα and inhibit its binding with a PGC-1α-derived peptide as measured in a FRET assay format ($IC_{50} = 0.19\ \mu M$) and has similarly served as a useful tool for structural studies.[33] Thiadiazoloacrylamide **4** (XCT790) was identified as a selective inverse agonist with potent cellular activity in a Gal4-ERRα transfection assay ($IC_{50} = 0.37\ \mu M$)[37] and has

served to help elucidate the role of ERRα signaling in vitro.[18,38] However, no information has been presented to date describing the pharmacological effects of an ERRα ligand in an in vivo metabolic model.

A series of diaryl ether-based thioazolidinediones was identified that function as potent and selective inverse agonists of ERRα in in vitro biochemical assays. The development of this series has culminated in the identification of **29**, whose favorable pharmacokinetic properties have allowed for the evaluation of pharmacological properties associated with selective ERRα modulation in vivo. Herein, the discovery and development efforts leading to **29** are described, along with structural studies that elucidate its binding mechanism. Finally, the efficacy of **29** in models of obesity and overt diabetes and its pharmacokinetic profile are presented, which support its further development as a novel antidiabetic agent.

Chemistry

A high-throughput binding assay using Thermofluor technology[39] was carried out with the LBD of ERRα in order to identify functionally unbiased ligands for this orphan receptor. From this screen, several members of a series of alkylidenyl diaryl ethers **A** (Figure 2) were identified as having modest receptor affinity. Functional activities of these screening hits were determined using a time-resolved fluorescence resonance energy transfer (TR-FRET) assay, in which compounds were tested for their abilities to inhibit the binding of a coactivator polypeptide derived from hSRC2. Since functional activities were found to generally correlate with binding, this assay was subsequently used for SAR development and series optimization. Expansion of the original Knoevenagel condensation library with a broad range of carbon acids revealed a clear preference for analogues derived from heterocyclic carbon acids, of which 2,4-thiazolidinedione (TZD) conferred particularly significant activity. Thus, from the initial screening campaign, nitroaryloxyphenyl TZD **5** and cyanoaryloxyphenyl TZD **6** (IC_{50} of 0.27 and 0.47 μM, respectively) served as validated hits for further hit-to-lead optimization studies.

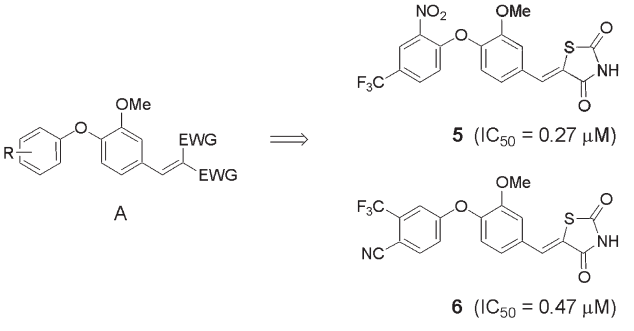

Figure 2. Knoevenagel-derived HTS hits.

Target compounds **D** were readily synthesized by condensing 2,4-thiazolidenedione with aryloxybenzaldehydes **C**. These in turn were prepared by a thermal S_NAr reaction between phenolic aldehydes and electron poor aryl fluorides **B** (Scheme 1). It was possible to effect the TZD condensation reaction under a variety of reaction conditions, many of which are exemplified in the Experimental Section.

Cyanoaryloxyphenyl analogue **6** served as a reference compound for the evaluation of SARs of the central vanillin-derived ring (B-ring). Simple substituent variations were explored (Table 1), which revealed a limited tolerance for modifications in this portion of the molecule. Removal of the R^3 methoxyl group (**7**) or replacing it with a methyl substituent (**8**) led to a slight decrease in inhibitory activity; increasing its size to ethoxyl (**9**) further attenuated activity. Likewise, translating the methoxyl group to the R^2 position (**10**) or incorporating an additional methoxyl group at R^5 (**11**) led to reductions in activity. A more significant loss of activity resulted from a replacement of the anisole ring with a naphthylene system (**12**). A variety of alternative substituents were evaluated in this central ring, none of which afforded an enhancement in activity relative to reference anisole **6** (data not shown). These results are consistent with previous findings from thiadiazoleacrylamide **4** lead validation studies,[37] wherein the vanilloid ring system appeared to be "beneficial for ERRα activity". The structural basis for the somewhat privileged nature of this core with respect to the present series later became apparent from cocrystallographic analysis of a lead analogue (**29**), which revealed the receptor interactions with which this ring is engaged (vide infra).

An investigation of the SAR of the terminal aryl C-ring (Table 2) supported a preference for an electron poor carbocyclic system in this portion of the molecule. Substituted pyridyl rings, for example, were essentially devoid of activity (data not shown). As observed in the FRET assay, the presence of a nitro substituent, irrespective of its ring position, appeared

Table 1. B-Ring Substituent Effects on ERRα Affinity

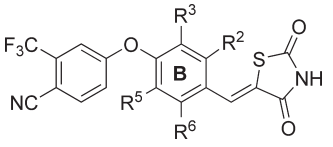

compd	R^2	R^3	R^5	R^6	FRET IC_{50} (μM)
6	H	OMe	H	H	0.47 ± 0.06
7	H	H	H	H	0.72 ± 0.11
8	H	Me	H	H	0.8 ± 0.11
9	H	OEt	H	H	0.35 ± 0.04
10	OMe	H	H	H	0.73 ± 0.11
11	H	OMe	OMe	H	1.8 ± 0.25
12	CH=CH	CH=CH	H	H	2.6 ± 0.56

Scheme 1. Synthesis of Arylidenyl Thiazolidenediones **D**[a]

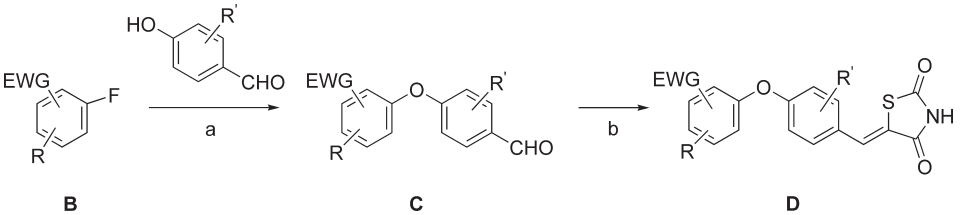

[a] Reagents and conditions: (a) K_2CO_3, DMF, 80−140 °C; (b) 2,4-thiazolidenedione, NH_4OAc, HOAc, 105 °C.

Table 2. C-Ring Substituent Effects on ERRα Affinity

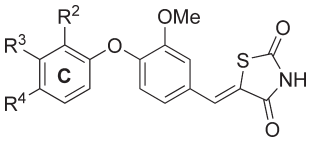

compd	R^2	R^3	R^4	FRET IC_{50} (μM)	two-hybrid IC_{50} (μM)
5	NO_2	H	CF_3	0.27 ± 0.004	3.6
13	NO_2	H	H	0.29 ± 0.05	>10
14	NO_2	H	CO_2Me	0.47 ± 0.06	>10
15	NO_2	H	CN	1.1 ± 0.27	>10
16	H	CF_3	NO_2	0.28 ± 0.04	5 ± 2.1
17	CN	H	NO_2	1.0 ± 0.08	
18	CN	H	H	2.4 ± 0.45	
19	CN	H	CN	0.5 ± 0.1	
20	CN	H	CF_3	0.24 ± 0.03	4.5
21	Cl	H	CO_2Me	0.047 ± 0.007	5.9 ± 2.5
22	Cl	H	CF_3	0.165 ± 0.02	2.3
23	Cl	H	CN	0.54 ± 0.09	>10
24	Br	H	CO_2Me	0.08 ± 0.01	3.4
25	Br	H	CF_3	0.14 ± 0.02	2.7
26	Br	H	CN	0.72 ± 0.09	6.3
27	CF_3	H	CO_2Me	0.016 ± 0.002	1.5
28	CF_3	H	CF_3	0.036 ± 0.005	>10
29	CF_3	H	CN	0.04 ± 0.015	0.6 ± 0.21
30	CF_3	H	H	0.068 ± 0.009	0.7 ± 0.2
31	CO_2Me	H	CF_3	0.07 ± 0.013	9.3
32	H	CF_3	CO_2Me	0.057 ± 0.006	>10
6	H	CF_3	CN	0.47 ± 0.014	>10
33	H	Me	CN	0.89 ± 0.16	>10
34	Me	H	CN	0.64 ± 0.09	
35	H	CN	CN	0.22 ± 0.05	6.9 ± 3.3
36	H	Cl	CN	1.3 ± 0.20	
37	H	H	CN	1.0 ± 0.22	
38	CH=CH	CH=CH	CN	0.062 ± 0.009	2.3
39	CH=CH	CH=CH	CO_2Me	0.013 ± 0.002	0.09 ± 0.03
40[a]	H	CF_3	CO_2Me	1.2 ± 0.22	

[a] Reduced analogue (saturated olefin).

to impart a threshold level of activity ($IC_{50} \geq 0.25\,\mu M$), which was not further increased by the incorporation of additional C-ring substituents. Thus, deletion of the 4-trifluoromethyl group (**13**) or replacement of it with a methyl carboxylate functionality (**14**) provided analogues with inhibitory activities comparable to that of initial hit **5**, whereas 4-cyano substitution (**15**) led to diminished activity. The isomeric 3-trifluoromethyl analogue **16** was also equipotent with **5**. Similarly, the 2-cyano-4-nitrophenyl derivative **17** was equipotent with its inverse regioisomer, 2-nitro-4-cyanophenyl analogue **15**.

In the absence of the C-ring nitro functionality, the contributions of additional ring substituents became somewhat more discernible. Compared with 2-nitro analogue **13**, the corresponding cyano derivative (**18**; $IC_{50} = 2.4\,\mu M$) was almost 10-fold weaker in inhibitory potency. However, incorporation of an additional cyano group at the 4-position (**19**) restored much of this activity; a 4-trifluoromethyl group (**20**) further increased inhibitory activity back to that of **5**.

Chloro (**21**−**23**) and bromo substituents (**24**−**26**) were found to be effective replacements for the 2-nitro substituent, while replacement with a 2-trifluoromethyl group provided generally improved potencies (**27**−**30**). Particularly potent inhibitory activities were observed with those compounds additionally bearing a methyl ester at the 4-position (**21**, **24**, and **27**; $IC_{50} = 0.047, 0.08$, and $0.016\,\mu M$, respectively), though this did present an unsuitable metabolic liability. While the corresponding acids (not shown) were found to be inactive in this assay, the ester functionality of **27** could be replaced by a nitrile with only a modest decrease in inhibitory activity (**29**; $IC_{50} = 0.04\,\mu M$). However, other 4-cyano analogues (**15**, **19**, **23**, **26**, **6**, **33**−**37**) proved to be significantly less active, a finding suggestive of a particularly favorable binding interaction that is optimally accessed by the 2-trifluoromethyl substituent. Among regioisomeric pairs in which this substituent was transposed to the 3-position, the 2-isomer was significantly more potent. Thus, ester **27** was some 3.5-fold more potent than **32** in the FRET assay; the difference was even more pronounced (> 10-fold) between the regioisomeric nitriles **29** and **6**. In addition, methyl analogues (**33** and **34**) proved less active than the corresponding trifluoromethyl derivatives (**6** and **29**, respectively), presumably reflecting favorable electronic and/or lipophilic contributions from the latter functionality.

The beneficial effects imparted by 2-trifluoromethylphenyl based C-rings were also conferred by (naphth-1-yl)-derived C-rings, as evidenced by analogues **38** and **39**. Thus, nitrile **38** was found to be equipotent with its 2-trifluoromethylphenyl counterpart (**29**) in this assay. Similarly, esters **39** and **27** were equally potent inhibitors of coactivator peptide binding.

In order to assess the importance of the olefinic linkage between the TZD and B-rings, ester **32** ($IC_{50} = 0.057\,\mu M$) was subjected to conjugate olefin reduction using a cobalt-mediated borohydride reaction, as described by Tanis.[40] The resulting

alkyl TZD (**40**; $IC_{50} = 1.2\,\mu M$) exhibited a 20-fold reduction in inhibitory activity, thus demonstrating a requirement for an unsaturated connectivity between these two ring systems. Again, the basis of this structural requirement for the series became readily apparent from the cocrystallographic structure of **29** with ERRα (vide infra).

Compounds were also evaluated in a two-hybrid luciferase reporter assay to determine their inhibitory effects in a cellular system. As can be seen in Table 2, inhibitory potencies in this assay did not correlate well with those observed in the coactivator binding assay, perhaps reflecting differences in cell permeabilities among series analogues. Thus, while compounds that were only weakly active in the former assay ($IC_{50} > 0.5\,\mu M$) also proved to be inactive in the two-hybrid format, several compounds exhibiting quite potent inhibition of coactivator peptide binding were essentially devoid of activity in this cellular assay (**21**, **28**, **31**, and **32**, for example). However, three compounds exhibited especially potent activities in both assays (**29**, **30**, and **39**); these and other selected analogues were further profiled for microsomal stabilities and their potential for cytochrome P450 (CYP) interactions with 3A4 and 2D6 isozymes (Table 3). As anticipated, series esters (**21**, **27**, and **39**) were metabolically unstable when incubated with human, mouse, or rat liver microsomes, whereas nitrile **29** and chlorobenzotrifluoride **22** proved quite stable against these microsomal preparations. The 4-unsubstituted benzotrifluoride **30** was somewhat less stable, suggesting that the 4-cyano and 4-chloro substituents (**29** and **22**, respectively) may block ring oxidation. Curiously, 4-bromo analogue **25** was markedly less stable than these compounds when incubated with mouse or rat microsomes.

In general, compounds of this class do not interfere with the activity of CYP 2D6, though some compounds were found to interact with the 3A4 isozyme at low micromolar levels. However, compounds **29** and **22** did not significantly inhibit either CYP isozyme ($IC_{50} > 10\,\mu M$).

Table 3. Cyp P450 Isozyme Interactions and Microsomal Stabilities of Selected Compounds

	IC_{50} (μM)		% remaining at 10 min		
compd	3A4	2D6	HLM	MLM	RLM
21	2.5	> 10	3	60	39
22	> 10	> 10	100	76	100
25	3.8	> 10	100	39	29
27	9.8	> 10	12	89	51
29	> 10	> 10	91	100	100
30	1.9	> 10	81	70	76
38	4.5	> 10	84	65	100
39	0.8	> 10	27	48	72

On the basis of its potent inhibitory activity against ERRα in both biochemical assays, its microsomal stability, and minimal CYP interactions, **29** was selected as a lead candidate for more extensive biochemical characterization and evaluation in vivo.

Selectivity Studies

The potential of **29** to interact with other nuclear receptors was investigated under a variety of assay conditions (Tables 4 and 5). A FRET assay similar to that described above for ERRα was developed to evaluate activity against ERRγ,[47] whereas a commercial fluorescence polarization assay (Invitrogen) provided a readout of activity against PPARγ.[48] Compared with its potent ERRα inhibitory activity ($IC_{50} = 0.04\,\mu M$), **29** proved much less potent (> 50-fold selectivity) at inhibiting coactivator peptide binding with ERRγ ($IC_{50} = 2.8\,\mu M$) and did not compete with PPARγ ligand binding at test concentrations up to 10 μM. Other nuclear receptors (LXRα, LXRβ, RARα) were similarly unaffected by **29**, as determined by corresponding coactivator binding competition assays ($IC_{50} > 8.3\,\mu M$) (Table 4).[49] Selectivity of **29** was also assessed against a panel of nuclear receptors in cellular reporter assays (Table 5), including all PPAR members and RXRα. At a test concentration of 15 μM, no functional activity was detected

Table 5. Activity of **29** in Functional and Cellular Reporter Assays against a Panel of Nuclear Receptors[a]

receptor	agonist[b] EC_{50} (μM)	antagonist[b] IC_{50} (μM)
ERRα		0.6
ERRγ		> 15
ERα[c]	> 15 (E2, 10 nM)	> 15
ERβ	> 15 (E2, 1.4 nM)	> 15
PPARα	> 15 (GW7647, 0.4 μM)	> 15
PPARγ	> 15 (rosiglitazone, 0.35 μM)	> 15
PPARδ	> 15 (GW0742, 0.3 μM)	> 15
RXRα	> 15 (bexarotene, 2.7 nM)	> 15

[a] Cellular reporter assays for a panel of nuclear hormones receptors. All assays utilize human receptor orthologues. Compound **29** was profiled against the ligand binding domain for a panel of nuclear hormone receptors assessing luciferase activity under the control of an artificial promoter. [b] Ligands in parentheses are the respective agonists for the nuclear receptors used in the antagonist mode. These ligands served as positive controls in the assay, and the determined EC_{50} values in the agonist mode are also reported within parentheses. GW7647 = 2-[4-[2-[3-cyclohexyl-1-(4-cyclohexylbutyl)ureido]ethyl]phenylsulfanyl]-2-methylpropionic acid;[43] rosiglitazone = ((±)-5-[4-[2-[*N*-methyl-*N*-(2-pyridyl)amino]ethoxy]benzyl]thiazolidine-2,4-dione);[44] GW0742 = 2-[4-[2-[3-fluoro-4-(trifluoromethyl)phenyl]-4-methylthiazol-5-ylmethylsulfanyl]-2-methylphenoxy]acetic acid;[45] bexarotene = 4-[1-(3,5,5,8,8-pentamethyl-5,6,7,8-tetrahydro-2-naphthyl)ethynyl]benzoic acid.[46] [c] MCF7 proliferation assay.

Table 4. Activity of **29** in Binding and Functional Assays against a Panel of Nuclear Receptors

receptor	binding[a] IC_{50} (μM)	agonist,[b,c] EC_{50} (μM) (% control)	antagonist,[b,c] IC_{50} (μM)
ERRα			0.040
ERRγ			2.8
PPARγ	> 10		
ERα	2.2	0.9 (31%) (E2; 5.9 nM)	> 6.3
ERβ	0.55	1.6 (24%) (E2; 4.6 nM)	> 6.3
LXRα		> 8.3 (TO901317; 3.2 nM)	> 8.3
LXRβ		> 8.3 (TO901317; 4.7 nM)	> 8.3
RARα		> 8.3 (AM580; 4 nM)	> 8.3

[a] FP assay format. [b] TR-FRET assay. [c] Ligands in parentheses are the respective agonists for the nuclear receptors used in the antagonist mode. These ligands served as positive controls in the assay, and the determined EC_{50} values in the agonist mode are also reported in the parentheses. E2 = 3,17β-estradiol; TO901317 = *N*-(2,2,2-trifluoroethyl)-*N*-[4-[2,2,2-trifluoro-1-hydroxy-1-(trifluoromethyl)ethyl]phenyl]benzenesulfonamide;[41] AM580 = 4-[(5,6,7,8-tetrahydro-5,5,8,8-tetramethyl-2-naphthalenyl)carboxamido]benzoic acid.[42]

against any of these receptors. Furthermore, the ability of **29** to indirectly activate PPARγ was investigated by evaluating its effect on adipocyte differentiation in the murine pluripotent mesenchymal C3H10T1/2 cell line.[50] In contrast to rosiglitazone, **29** did not induce adipogenesis at the highest test dose (15 μM), as quantified by total triglyceride (data not shown).

Against the estrogen receptors ERα and ERβ, **29** was found to compete with ligand binding (IC_{50} of 2.2 and 0.6 μM, respectively)[48] but did not disrupt the 3,17β-estradiol (E2) mediated coactivator recruitment function of either receptor when tested at 6.3 μM.[49] In functional biochemical assays measuring the promotion of coactivator peptide recruitment, **29** behaved as a weak partial agonist, providing 30% (ERα) and 25% (ERβ) efficacy relative to estradiol (apparent EC_{50} values of 0.9 and 1.6 μM, respectively). However, **29** failed to induce proliferation in MCF7 cells or antagonize the proliferative effect of E2 on these cells (an effect that is predominantly mediated by ERα receptor activation). Likewise, **29** failed to activate ERβ or antagonize the stimulatory effects of E2 on this receptor in cellular reporter assays (Table 5). The lack of functional activation of the ERβ receptor was also confirmed in vivo. In a chronic efficacy study in the male ZDF model (vide infra), prostate weight, which is a sensitive maker for estrogenic activity in rodent models,[51] was unaffected following 28 days of dosing. Thus, with respect to nuclear receptor interactions, **29** potently and selectively inhibits the functional activity (coactivator recruitment) of ERRα. The modest activity that was detected in vitro against ERα and ERβ at > 10-fold higher concentrations does not appear to be functionally consequential in vivo.

Compound **29** was also evaluated for selectivity in a general binding screen (Cerep) against a standard panel of 51 receptors and ion channels. At a test concentration of 10 μM, **29** did not inhibit paradigm compound binding greater than 40%, with the sole exception of the chloride channel, against which picrotoxin binding was partially inhibited (60%). Similarly, against a standard kinase panel of 50 enzymes (Invitrogen), **29** showed no significant inhibitory activities (> 30%) at a test concentration of 20 μM.

Structural Studies

Previously described structural studies have provided mechanistic insight into the constitutive activity of ERRα and the conformational changes that occur within its LBD upon coactivator binding. The first published X-ray crystal structure of the ERRα LBD was obtained in complex with a coactivator peptide derived from PGC-1α and localized the binding interface to a region of the LBD comprising helix H12 together with helices H3 and H4 (so-called "coactivator groove").[32] A subsequent structure of the LBD (containing a C325S mutation to facilitate protein purification and crystallization) in complex with synthetic inverse agonist **3** provided evidence of the significant conformational shifts that must occur in order to accommodate the binding of this ligand.[33] Most notably, H12 is displaced from its agonist position and subsequently fills the coactivator groove of the AF2 domain.

We have obtained an X-ray crystal structure (PDB code 3K6P, 2.0 Å resolution) of the LBD of ERRα (amino acids 289−519, Swiss-Prot P11474)[52] in complex with **29**, which provides further insight into the molecular basis of inverse agonism (Figure 3). The putative ligand-binding pocket of the receptor undergoes significant conformational changes and

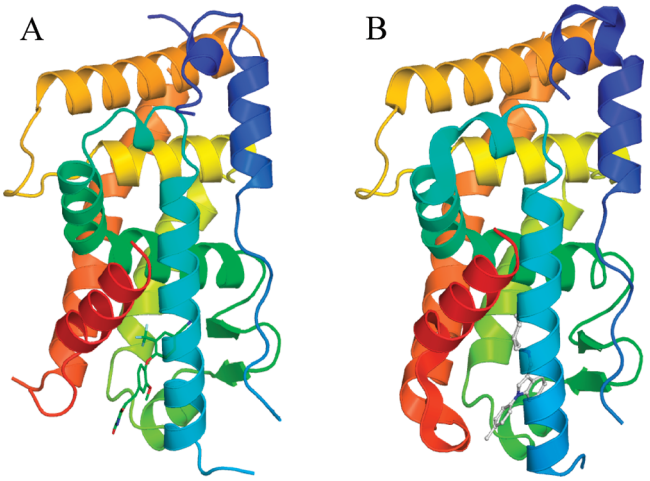

Figure 3. Ribbon drawing of the crystal structure of ERRα LBD. (A) ERRα in complex with compound **29**. Color is ramped from the N terminus in blue to the C terminus in red. Compound **29** is depicted in green with atoms colored by element: nitrogen (blue), oxygen (red), sulfur (yellow), and fluorine (cyan). (B) ERRα in complex with compound **3**.[33] Figures 3 and 4 were generated by PyMOL (DeLano, W. L. *The PyMOL Molecular Graphics System*; **2002**).

side chain rotations (for example, Phe328) in order to accommodate **29**, similar to those reported with **3**.[33] Relative to the apo-ERRα structure (agonist conformation), in addition to the aforementioned displacement of helix 12, a major shift of the main chain was observed at the base of helix 11 and the intervening loop between helices 11 and 12. The AF2 domain, whose native conformation is responsible for transducing the constitutive activity for the receptor, is now largely occupied by H12 in much the same fashion as was observed with **3**.[33]

As indicated above, SAR studies revealed that the vanilloid ring system is highly sensitive to substituent variability. The diaryl ether portion of the molecule is embedded in a hydrophobic region of the AF2 domain wherein it forms significant van der Waals interactions. Both the vanilloid and terminal phenyl rings flank Phe328 to participate in edge-to-face π-interactions with this critical residue. In addition, the base of helix 11 is further translated away from helix 3 than in the apo- and **3**-cocomplex structures, thus creating a binding pocket for **29** that extends further into the protein interior. This positions the vanilloid ring in proximity to Phe495 (base of helix H11), with which it likely engages in van der Waals stabilization interactions. This differs somewhat from the conformation of cocomplex **3**, wherein a π-stacking interaction between Phe495 and Phe328 was induced; in complex with **29**, the vanilloid ring intercedes in this interaction by further displacing Phe495 (Figure 4). Also noteworthy is the highly lipophilic pocket into which the 2-trifluoromethyl substituent (C-ring) extends, a region bounded by several hydrophobic side chain residues (Leu398, Val491, Leu405, Leu401, Val366, Met362, Phe495, and Met506). Thus, the lipophilic complementarity of the 2-CF_3 group with respect to this receptor region likely accounts for the increased potency of analogues bearing this functionality, particularly compared with corresponding methyl-substituted derivatives.

As a compound class, thiazolidinediones (TZDs) are well recognized as agonists of the peroxisome proliferator-activated receptor, PPARγ, which function in vivo as insulin sensitizers and have been developed for the treatment of type 2 diabetes.[53] These TZDs are saturated at the 5-position and are

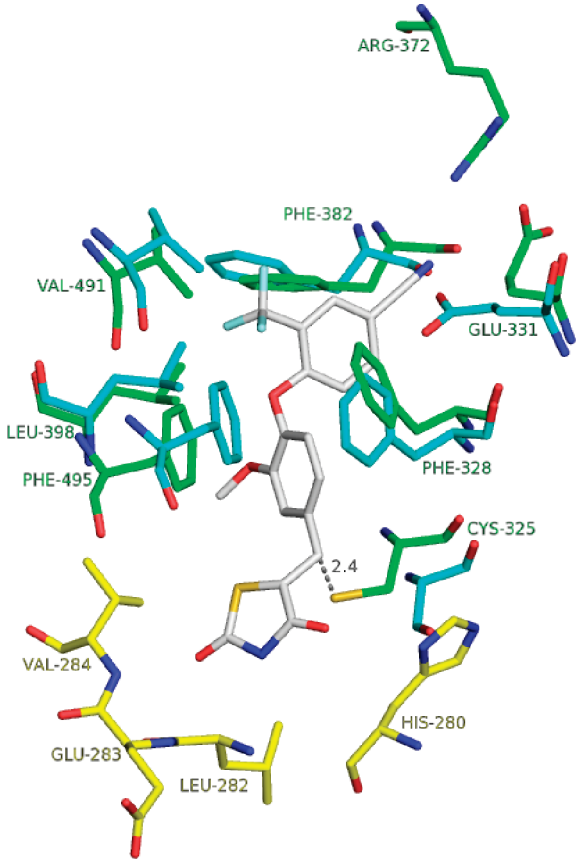

Figure 4. Comparison of side chain orientations between ERRα-**29** and ERRα-**3**[33] structures. Residues from the ERRα-**29** complex are shown in green; residues from the ERRα-**3** complex are shown in cyan. Compound **29** is depicted in gray. ERRα residues from a crystal packing molecule are shown in yellow. Atoms are colored by element: nitrogen (blue), oxygen (red), sulfur (yellow), and fluorine (cyan).

substituted at this ring position with various 4-alkoxybenzylic groups. Importantly, saturation at this position confers a bent conformation that directs the acidic TZD ring system such that it engages in multiple direct H-bonding interactions (and induces additional secondary H-bonding interactions) with specific receptor residues located deep within the LBD of PPARγ.[54] In stark contrast, the thiazolidinedione headgroup of **29** does not participate in such interactions with ERRα but rather is oriented away from the interior of the protein. It extends toward the protein surface where, as a result of crystal packing, it interacts with N-terminal residues (main chain amino groups of Val284, Glu283, and His281; side chain NE2 of His280) of a second ERRα-symmetry crystallization molecule.

Furthermore, a critical thioether bond is formed between Cys325 of helix H3 and **29** via conjugate addition to the α,β-unsaturated TZD system. The unavailability of this interaction with saturated analogues such as **40** provides a probable explanation for the attenuated activities of such derivatives against ERRα. Likewise, the olefinic geometric constraints of these ligands preclude an interaction with PPARγ in the typical TZD fashion and likely contributes to the observed selectivity of this series as measured against this NR.

Competition binding experiments were carried out in order to investigate the reversibility of this covalent complex formation. Incubation of the LBD of ERRα with **29** (2 equiv) resulted in a time-dependent increase in the complex concentration, as determined by LCMS analysis (ESI^+ TOF). The protein molecular weight increased by 421 Da (equal to the mass of **29** + 1 amu), and no additional adducts with the protein were observed (Figure 5). Upon complete ERRα-**29** complex formation (~1 h), competing ligand **27** was added (20 equiv relative to **29**), and a new complex, ERRα-**27** (protein + 453 Da + 1 amu), formed at the expense of the original ERRα-**29** complex. The time-dependent formation of this new complex served as a surrogate for the disassociation of the ERRα-**29** complex, whose apparent half-life in vitro was estimated to be ~18 h. Furthermore, recovered **29** was determined to be structurally intact; hence, its dissociation from ERRα was not a result of degradative fragmentation. Thus, the association of **29** with ERRα results in a covalent but slowly reversible complex, whose formation induces significant conformational changes in the AF2 domain and thereby precludes coactivator protein binding.

Pharmacokinetic Studies

In order to assess the pharmacokinetic behavior of this compound class, **5**, **38**, and **29** were selected for PK studies in Sprague−Dawley rats. At doses of 2 mg/kg (iv) and 10 mg/kg (po), all three analogues exhibited favorable pharmacokinetic profiles with high oral bioavailabilities (> 70%) (Table 6). In the case of **5**, a maximal plasma concentration of 6.4 μg/mL was realized ~2 h after oral dosing (t_{max}), which remained at this level for 6 h, then slowly decreased over the remaining study period. Thus, an estimated terminal elimination half-life ($t_{1/2}$) of 9.8 h reflects a prolonged plasma stability and low clearance rate (1.0 (mL/min)/kg). A low clearance rate was also observed with **38** (Cl = 0.5 (mL/min)/kg), whose maximal plasma concentration following oral dosing (C_{max} = 12.6 μg/mL) was twice that of **5**. Again, plasma levels indicated a slow absorption phase (t_{max} = 5.5 h) followed by a prolonged terminal elimination phase ($t_{1/2}$ = 13 h). These results are consistent with the high metabolic stabilities observed in vitro in the presence of liver microsomal preparations. Absorption of **29** following oral administration was also moderately slow (t_{max} = 3 h), leading to a maximal plasma concentration of 6.3 μg/mL, which then decreased in a monophasic manner ($t_{1/2}$ = 7.8 h). The oral bioavailability of **29** was determined to be 78% in the rat.

Further evaluation of **29** in the mouse, dog, and monkey revealed similarly favorable PK profiles (Table 6). Again, high (> 90%) oral bioavailabilities were observed in these species. In the mouse, biphasic absorption/elimination phases were observed following both iv (t_{max} = 0.5 and 2 h) and po (t_{max} = 0.5 and 4 h) dosing. This is possibly indicative of compound redistribution by enterohapatic recirculation, which is reflected in the particularly high oral bioavailability (147%). High serum concentrations of **29** (C_{max} = 6.8 μg/mL at 0.5 h; C_{max} = 5.4 μg/mL at 4 h) were maintained throughout the study (7 h); the terminal elimination is roughly estimated ($t_{1/2}$ = 2.5 h) (Table 7). In the dog, an even higher serum concentration was obtained (C_{max} = 14.3 μg/mL; t_{max} = 5.5 h) with a 5 h terminal elimination ($t_{1/2}$). In the monkey, a lower maximal serum concentration was achieved (C_{max} = 4.2 μg/mL); however, the half-life in serum was significantly longer ($t_{1/2}$ = 12.8 h) resulting in measurable drug levels at 72 h. Thus, exposures of **29** in each of the four species examined were considerable ($AUC_{0-n} \approx 30-220$ μg·h/mL).

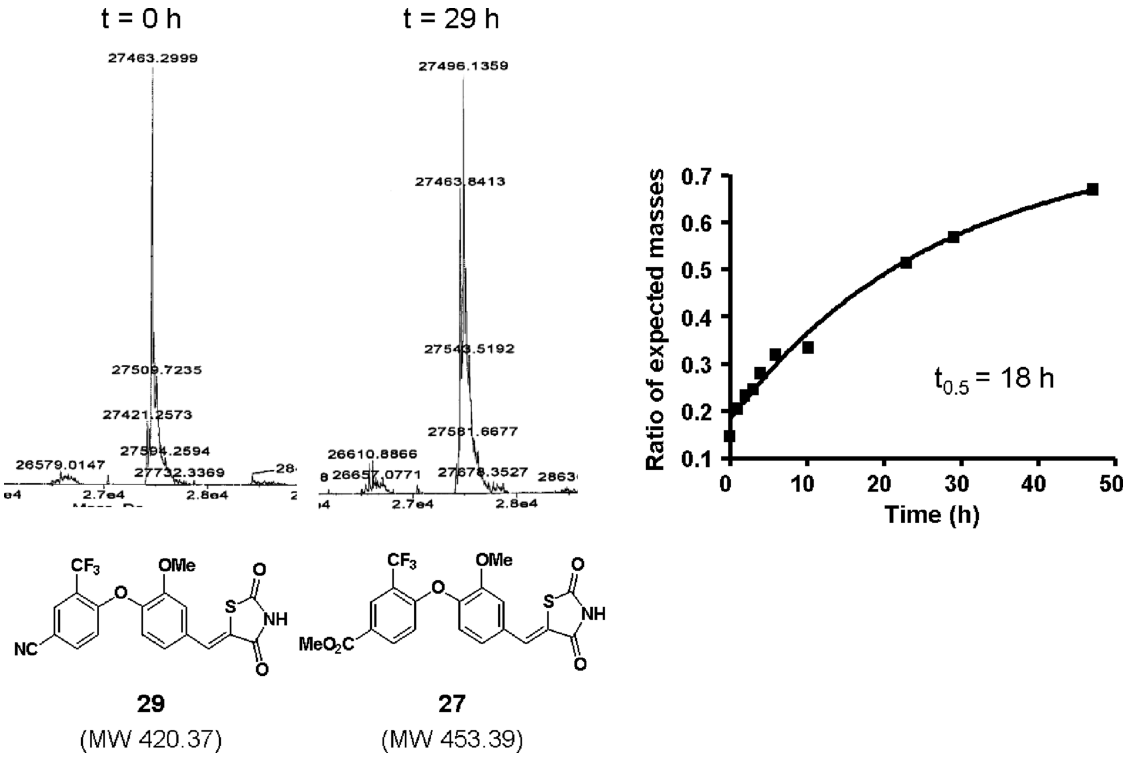

Figure 5. Monitoring the dissociation of the ERRα-**29** complex by LCMS. Addition of excess competition ligand **27** resulted in displacement of **29** by **27** and to a corresponding change in the molecular weight of the protein by +33 amu (the difference between **29** and **27**). The apparent half-life of the ERRα-**29** complex in vitro was approximately 18 h.

Table 6. Pharmacokinetic Parameters for **5**, **38**, and **29** after iv and po Administration to Adult Male Sprague Dawley Rats

	intravenous dosing[a]			oral dosing[b]				
compd	Cl ((mL/min)/kg)	V_{ss} (L/kg)	$t_{1/2}$ (h)	C_{max} (μg/mL)	t_{max} (h)	AUC_{0-24} (μg·h/mL)	$t_{1/2}$ (h)	F (%)
5	1.0	0.54	7.8	6.3[c]	3.5[c]	96.8[c]	9.5[c]	138[c]
38	0.5	0.39	9.2	12.62	5.5	213	13	74
29	1.0	0.80	6.9	6.3	3	84.4	7.8	77

[a] 2 mg/kg, $n = 4$ animals per group. [b] 10 mg/kg, $n = 4$ animals per group. [c] 5 mg/kg, $n = 4$ animals per group.

Table 7. Pharmacokinetic Parameters for Compound **29** after iv and po Administration to Adult Male CD-1 Mice, Adult Female Beagle Dogs, and Adult Female Cynomolgus Monkeys

	intravenous dosing[a]			oral dosing[b]				
species	Cl ((mL/min)/kg)	V_{ss} (L/kg)	$t_{1/2}$ (h)	C_{max} (μg/mL)	t_{max} (h)	AUC_{0-48} (μg·h/mL)	$t_{1/2}$ (h)	F (%)
mouse	5.01	1.16	2.7	6.8	0.5	30.3[c]	2.5	147
dog	0.87	0.32	5.0	14.3[d]	4.5[d]	228.2[d]	5.5[d]	91[d]
monkey	0.72	0.78	12.8	4.2	7	71.8[e]	13.9	118

[a] 2 mg/kg, $n = 3$ animals per group. [b] 10 mg/kg, $n = 3$ animals per group. [c] AUC_{0-7}. [d] One dog was not included in the calculation of mean parameters because of an emetic episode. [e] AUC_{0-72}.

Pharmacological Studies

In light of the lean phenotype of the ERRα$^{-/-}$ mouse and its resistance to high-fat diet-induced obesity, the effects of **29** in animal models of obesity and diabetes were investigated. AKR/J mice are a polygenic model of diet-induced obesity characterized by hypertriglyceridemia and hyperinsulinemia.[55] The effects of **29** (3 and 30 mg/kg, b.i.d.) via oral administration in AKR/J mice maintained on a high-fat diet were evaluated in a 5-day efficacy study. As shown in Table 8, significant weight loss (5%) and reductions in food intake (23%) were observed in animals treated at the higher dose compared with vehicle-treated controls. The reduction in body weight was accompanied by a selective decrease in body fat without a change in lean mass. At this same dose, **29** reduced circulating insulin levels by 67% without concomitant changes in fed glucose levels, indicating an improvement of peripheral insulin sensitivity. In addition, triglyceride levels were reduced by ~50%. Trends toward lower FFA and higher ketone (3-hydroxybutyrate) levels were observed at this higher dose; however, these did not reach statistical significance. No apparent toxicities or adverse effects were observed at either dose in this study.

Analogous results were observed in a subchronic model of diet-induced obesity and insulin resistance, in which C57BL/6 mice under a high-fat diet were treated with **29** (10 and 30 mg/kg, q.d.) for 15 days. When placed on such a diet, these mice develop hyperglycemia, hyperinsulinemia, and impaired glucose tolerance[56] and their serum chemistries exhibit elevated levels of cholesterol, triglycerides, and FFAs.[57] Interim analysis

Table 8. Effects of **29** on Male AKR/J Mice (Body Composition and Metabolic Parameters)[a]

parameter	vehicle	**29** (3 mg/kg)	**29** (30 mg/kg)
body weight Δ (g) (day 4 to day 0)	−0.89 ± 0.15	−1.09 ± 0.27	−1.65 ± 0.25*
food intake (g/day)	8.7 ± 0.2	8.0 ± 0.3	6.7 ± 0.4
total body fat (g)	3.96 ± 0.35	3.87 ± 0.29	2.7 ± 0.2**
lean mass (g)	20.5 ± 0.4	20.2 ± 0.3	20.0 ± 0.2
% body fat	13.5 ± 1.2	12.7 ± 0.8	9.3 ± 0.6**
insulin (ng/mL)	8.5 ± 0.9	9.6 ± 1.5	2.8 ± 0.8**
triglyceride (mg/dL)	159.1 ± 19.5	160.0 ± 18.9	80.0 ± 9.8**
glucose (mg/dL)	163.9 ± 6.8	165.0 ± 5.0	185.0 ± 10.01
FFA (mM)	0.53 ± 0.04	0.59 ± 0.07	0.41 ± 0.05
3-hydroxybutyrate ($\times 10^{-5}$ M)	8.9 ± 0.8	8.3 ± 0.9	12.6 ± 1.8

[a] (*) $p < 0.05$. (**) $p < 0.01$. Results are reported as the mean and the standard error of the mean for $n = 10$.

Table 9. Effects of **29** on Male C57BL/6 Mice (Metabolic Parameters, Day 10; OGTT, Day 14)[a]

parameter	vehicle (high fat diet)	vehicle (low fat diet)	**29** (10 mg/kg)	**29** (30 mg/kg)
insulin ng/mL	2.5 ± 0.4	1.3 ± 0.1*	1.4 ± 0.1*	1.3 ± 0.05*
triglyceride (mg/dL)	72 ± 3.4	67 ± 0.9	58 ± 0.5**	59 ± 1.7*
glucose (mg/dL)	192 ± 13	181 ± 8.1	176 ± 14	174 ± 6.8
FFA (mM)	0.64 ± 0.1	0.49 ± 0.04	0.38 ± 0.03*	0.40 ± 0.04*
OGTT glucose AUC_{0-60} (mg·min/dL)	17043 ± 628	13768 ± 424	15077 ± 673	14425 ± 603*

[a] (*) $p < 0.05$. (**) $p < 0.01$. Results are reported as the mean and the standard error of mean for $n = 8$. Glucose load for the OGTT was 1 g/kg.

of blood samples (day 10) revealed that both doses of **29** were equally effective at reducing circulating insulin, free fatty acid, and triglyceride levels (46%, 18%, and 40%, respectively) compared to vehicle-treated animals (Table 9). These reduced levels, which were maintained throughout the remainder of the study, were equal to or lower than those of vehicle treated mice maintained on a low fat diet (chow diet). No changes in food intake, body weight, or body composition were noted in this study. No apparent toxicities, adverse events or changes in organ weights were observed, with the exception of a dose-dependent increase in liver weight (26% at 30 mg/kg) and elevated liver triglyceride levels (2-fold and 3-fold at 10 and 30 mg/kg, respectively). Despite the increased triglycerides, AST and ALT levels were unchanged and other clinical chemistries were normal. An oral glucose-tolerance test (OGTT) performed at day 14 of this study revealed improved glucose handling in treated animals. At the start of this test, those mice treated with 30 mg/kg **29** presented fasting glucose levels that were 20% less than vehicle controls (Figure 6). Thirty minutes following a 2 g/kg oral glucose gavage, relative serum glucose levels were reduced by 17% and 24% at the 10 and 30 mg/kg doses, respectively. At 60 min, 12% and 15% reductions in total serum glucose (AUC_{0-60}) were measured at these respective doses (Figure 6 and Table 9).

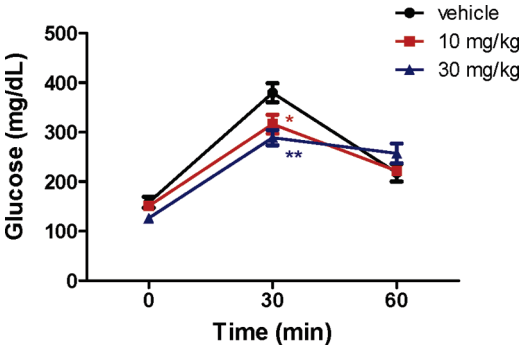

Figure 6. Effect of **29** on glucose excursion in an OGTT in male C57BL/6 mice after 14 days of treatment.

Microarray gene analysis was performed on liver-, muscle-, and adipose-extracted RNA for the vehicle and treatment animals (10 mg/kg cohort) in order to obtain mechanistic insights for the observed improvements in metabolic end points resulting from administration of **29**. Interestingly, with respect to this microarray analysis, the liver proved to be the most responsive tissue following treatment. Gene ontology clustering of differentially regulated transcripts enriched terms associated with fatty acid metabolism, synthesis and oxidation (see Supporting Information Table 1). Closer examination revealed that many of these genes contain estrogen-related receptor response elements within their promoter sequences. Particularly enriched were genes involved in lipid transport and mitochondrial function, several of which have been previously reported to be regulated by ERRα, such as *ATP5A1*, *Acadm*, and *IDH3A*. In addition, the *ACOX1* and *ADIPOQ* genes, which are known to be regulated by PPARs, were affected by treatment with **29** (*ACOX1*, *PPARA*, and *PPARG* contain ERREs within their promoter regions). These results suggest that there are likely overlapping cistromes for ERRα and PPARs in hepatic tissue and that ERRα may regulate PPAR-dependent signaling pathways in this tissue.

Genetic deletion of ERRα has a direct effect on the expression levels of hepatic gluconeogenic genes including *PCK1* and *GlyK*. A comparative study was performed to evaluate the expression levels of these genes (along with *Acadm*) in the ERRα knockout mouse versus the wild type, each of which was maintained on a high-fat diet. *GlyK* and *Acadm* expression levels were moderately increased in the knockout animals (Supporting Information Table 2), whereas a trend toward reduced expression of *PCK1* was observed in these animals ($p = 0.06$). In wild type animals treated with **29**, similar effects on the expression of these genes were observed, in terms of both magnitude and direction of response. Furthermore, treatment of the knockout mice with **29** did not alter these expression levels. Thus, with respect to hepatic gene expression, pharmacological treatment in these animals appears to mimic certain aspects of the phenotype of the ERRα knockout animals. Transcriptional profiling of the skeletal muscle and adipose tissue revealed a much smaller number of genes affected by treatment with **29**; therefore, no significant gene ontology terms from these tissues were produced.

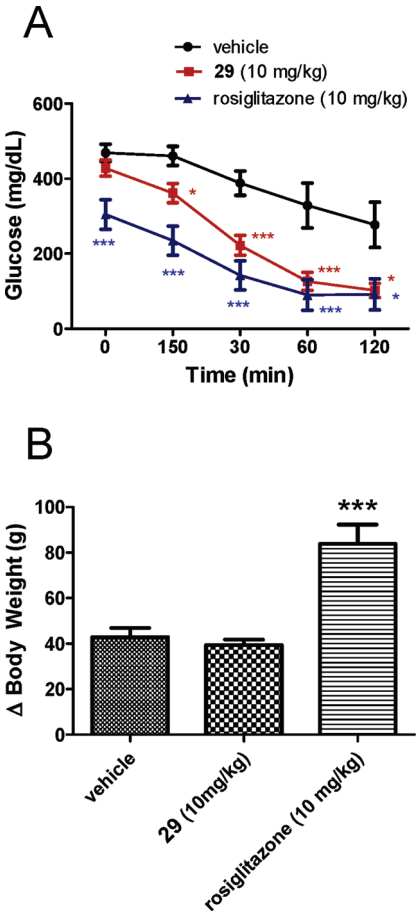

Figure 7. (A) Effect of **29** and rosiglitazone on an insulin tolerance test and in ZDF rats after 12 days of treatment. (B) Effect of **29** and rosiglitazone on body weight after 11 days of treatment.

The finding that *Acadm* was not differentially regulated in adipose tissue contrasts with the previous description of the ERRα knockout mouse (maintained on a standard chow diet), whose adipose *Acadm* expression levels were found to be up-regulated.[30] However, in our laboratories, analysis of adipose and muscle tissues from ERRα knockout mice that have been maintained on a high-fat diet for 13 weeks revealed no changes in the expression levels of this gene. This apparent inconsistency in phenotype may be the result of diet-induced compensatory mechanisms that come into operation in the absence of ERRα expression in these tissues. Alternatively, this may reflect a fundamental difference between global receptor deletion and temporal, possibly tissue selective pharmacological receptor modulation.

The efficacy of **29** was further evaluated in an overtly diabetic rodent model with rosiglitazone as an active comparator. The Zucker diabetic fatty (ZDF) rat is a well established monogenic model of type II diabetes, arising from a mutated *fa* gene, which produces a truncated leptin receptor that cannot interact with the natural peptide hormone. This mutation results in a hyperphagic phenotype and causes the rodent to develop obesity, hyperlipidemia, fasting hyperglycemia, and type II diabetes. To assess the effects on insulin sensitivity, an insulin tolerance test was conducted following 12 days of oral administration of **29** (10 mg/kg). As shown in Figure 7A, following intraperitoneal delivery of insulin (3 U/kg), a marked decrease of plasma glucose levels was observed (relative to vehicle-treated animals) resulting in near normalization of these values.

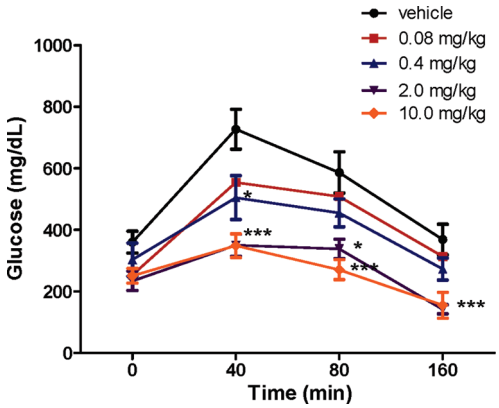

Figure 8. Effect of **29** on glucose excursion in an OGTT in male ZDF rats after 22 days of treatment.

The enhancement in insulin sensitivity afforded by **29** was comparable to that produced by rosiglitazone (10 mg/kg), although the former did not afford an improvement in the 4 h fasting glucose levels. Importantly, in contrast to rosiglitazone, which produced a dramatic increase in body weight (consistent with previous reports), **29** proved to be weight neutral (Figure 7B).

A follow-up study was conducted in the same model to address the effects of **29** on glucose clearance and to provide a PK/PD relationship for these effects (Figure 8). As shown in Table 10, following 14 days of oral administration of **29**, a dose-dependent reduction of fed glucose levels, triglycerides, and FFAs was observed that reached significance at the 10 mg/kg dose. At day 22 of the study, an OGGT revealed a dose-dependent reduction in glucose excursion that was maintained through 160 min. Moreover, significant reductions in the glucose AUC values were observed (−29% at 0.4 mg/kg, −48% at 2 mg/kg, and −52% at 10 mg/kg), indicating an improvement in glucose tolerance at all test doses. No changes in weight or epididymal fat pad were noted (data not shown). No apparent toxicities or adverse effects were observed for the treated animals at the end of the study. Drug exposures were also determined for a separate cohort of animals on day 22 following daily oral dosing (Table 11). Blood levels of **29** increased (t_{max} = 3−4 h) in a dose-dependent fashion to maximal concentrations (C_{max}) ranging from 0.08 to 9.3 μg/mL (0.08 and 10 mg/kg groups, respectively). Dose-linear exposures had also been attained, with $AUC_{(0-48h)}$ values ranging from 1.4 to 168 μg·h/mL. At a dose level of 2.0 mg/kg (C_{max} = 2.76 μg/mL; 6.6 μM), **29** was maximally effective with respect to the OGTT. These drug exposures are comparable to the concentration required to modulate the activity of the receptor in the cell based assay (Table 5).

Discussion

Previous biochemical, molecular, and genetic studies have demonstrated that ERRα is capable of modulating the transcription of a wide range of genes including key regulatory genes involved in lipid handling and metabolism (*ApoA-IV*, *Acadm*), mitochondrial respiration (OXPHOS genes), gluconeogenesis (*PCK1*), and glycolysis (*PDK*). However, ERRα is but one of several transcription factors feeding into a highly complex network of transcriptional activities that act in concert to meet the variable energy demands of an organism. Other nuclear receptors (ERRγ and PPARα, for example) share many of ERRα's cofactor interactions and gene targets,

Table 10. Effects of **29** on Male ZDF Rats (On Metabolic Parameters, Day 14; OGTT, Day 22)[a]

dose (mg/kg)	glucose (mg/dL)	triglycerides (mg/dL)	FFA (mM)	glucose AUC_{0-160} [b] (mg·min/dL)
vehicle	550 ± 49	522 ± 36	2.1 ± 0.2	86248 ± 8565
0.08	455 ± 68	544 ± 37	2.3 ± 0.2	70290 ± 7192
0.4	482 ± 53	486 ± 21	1.7 ± 0.2	64572 ± 6684*
2.0	416 ± 54	466 ± 29	1.5 ± 0.2	44672 ± 3559***
10.0	363 ± 60*	353 ± 38***	1.4 ± 0.3*	40998 ± 4118***

[a] (*) $p < 0.05$. (**) $p < 0.01$. (***) $p < 0.001$. Results are reported as the average and the standard error of mean for $n = 12$. [b] Glucose load for the OGTT was 2 g/kg.

Table 11. Pharmacokinetic Parameters for **29** after Multiple Oral Doses in Male ZDF Rats[a]

dose (mg/kg)	C_{max} (μg/mL)	AUC_{0-48} (μg·h/mL)	t_{max} (h)	$t_{1/2}$ (h)
0.08	0.08	1.4	4	9.8
0.4	0.33	6.8	4	11.3
2	2.76	58.9	2.7	10.1
10	9.3	168.3	4	7.9

[a] $n = 4$ animals per group.

thus providing overlapping and/or redundant pathways to support the maintenance of energy homeostasis. And so while the direct modulation of ERRα activity in a given cell or tissue type may lead to altered target gene transcriptions in vitro, an associated effect may not necessarily be phenotypically manifested in the whole animal because of differential tissue-selective regulatory activities of ERRα and/or functional input from compensatory mechanisms. Thus, the effects of global ERRα modulation in vivo have been difficult to predict up to this point.

The olefinic thiazolidinediones of the present series appear to function as selective modulators of ERRα in vitro. Olefinic TZDs have historically been found to exhibit activities across a broad range of therapeutic targets. As Michael acceptors, they are potentially susceptible to nonspecific reactions with proteins and may give rise to false-positive bioassay results, particularly in the context of HTS campaigns. Whereas such compounds have recently been described as problematic, pan assay interference compounds (PAINS),[58] the analogues described herein, do not appear to be promiscuous, based on preliminary selectivity screening data. Thus, representative analogues from this series (**5**, **23**, **29**) exhibit negligible off-target effects as measured against a general selectivity screening panel of receptors, ion channels, and enzymes and have also been shown to minimally affect other nuclear receptors including PPARγ, a well-established target of saturated TZDs. Selected compounds from this series were found to exhibit excellent pharmacokinetic properties in various animal species, and this has allowed us to examine the effects of ERRα modulation in vivo. In two mouse models of diet-induced obesity and in a rat monogenic model of type II diabetes, oral administration of **29** effects changes in body composition and serum chemistry that are consistent in certain respects with the phenotype presented by the ERRα-null mouse. In addition, this treatment afforded significant improvements in insulin sensitivity and glucose tolerance in these animals.

Serum triglyceride levels (TGs) in all models were significantly reduced in response to treatment with **29**, as were serum levels of free fatty acids (FFAs), though in the 5-day AKR/J study the latter reduction did not reach statistical significance. In the ERRα-null mouse, normal serum TGs and FFAs have been reported in animals maintained on a regular diet; however, corresponding levels in animals maintained on a high-fat diet were not reported.[30] Reduced expression of genes involved in dietary lipid processing has been observed in isolated enterocytes from ERRα-null mice, including *apoA-IV*, which was shown to be directly activated by ERRα/PGC-1α.[29] Gene expression profiling of hepatic tissue from C57BL/6 DIO mice treated with **29** showed a reduction in the expression of *apoA-IV*, while that of other apolipoproteins, including *apoC-II* and *apoC-III*, was increased. Most notably, clusters of genes involved in fatty acid oxidation (*Acadm*, *PPARA*, *ACOX1*), the tricarboxylic acid cycle (*IDH3A*, *IDH3B*), and insulin sensitivity (*ADIPOQ*) were affected with treatment. Thus, the improvement in triglyceride clearance may be the direct result of the augmentated hepatic fatty acid oxidation and enhanced mitochondrial function resulting from treatment with **29**. This would be consistent with studies in vitro that correlate alterations of these pathways with ERRα modulation. Perhaps the most significant finding presented herein is the effect of **29** on glucose handling and insulin sensitivity. The improvements in both of these parameters mirror the insulin-sensitive phenotype that has been observed in the ERRα-null mouse.[59] While the exact underlying mechanism(s) for these putative ERRα-related effects in vivo remains to be determined, one possible contributing mechanism may involve the increased hepatic fatty acid oxidation and concomitant clearance of circulating lipids, resulting in an indirect improvement of glucose tolerance and insulin sensitivity. However, the possibility cannot be excluded that additional unidentified mechanisms, functioning independently of ERRα modulation but not encompassed by our selectivity screens, may also be operational.

Mitochondrial dysfunction has been linked to the development of insulin resistance and diabetes; however, the role of ERRα in this pathophysiological condition has not been clearly defined. ERRα (constitutively active or acting in concert with PGC-1α) has been shown to be a positive regulator of the transcription of genes in the TCA cycle, oxidative phosphorylation, and mitochondrial transport in multiple cell types, in vitro.[60] Gene expression profiling of the ERRα KO mice has revealed only modest effects on the expression of ERRα target genes, implying that other transcription factors, including ERRγ, may act in concert with PGC-1 in the absence of ERRα.[61] Consistent with these findings, we observed known ERRα target genes to be similarly modestly up-regulated after treatment with **29**, i.e., TCA cycle genes (*IDH3A* and *IDH3B*), electron transport genes (*COX7B*, *COX6B1*), mitochondrial transport genes (*SLC25A5* and *SLC25A4*), and β-oxidation genes (*Acadm* and *HADHB*). Thus, selective ERRα ligands such as **29**, which up-regulates genes involved in mitochondrial biogenesis and respiratory capacity in vivo, may be expected to improve insulin sensitivity and glucose control in diabetics.

In summary, the effects of modulating ERRα function in animal models of obesity and diabetes were investigated through the use of the selective, orally bioavailable ERRα modulator **29**. In DIO mouse models and in a monogenic diabetic rat model, treatment with **29** led to the normalization of serum triglyceride and insulin levels as well as an improvement in

glucose tolerance. These results are consistent with the hypothesis that selective ERRα modulation can provide enhanced insulin sensitivity in vivo and lend support for the further development of such agents for the potential treatment of metabolic diseases such as type 2 diabetes.

Experimental Section

Reagents and solvents were obtained from commercial suppliers and used without further purification. Flash chromatography was performed with either glass columns packed with silica gel 60 (230−400 Mesh, EM Science) or prepacked silica gel cartridges (Redisep or Analogix) using a Teledyne-Isco CombiFlash Companion chromatography system. Radial chromatography was performed on a Cyclograph centrifugal chromatography system (Analtech, Inc.) with silica gel GF rotor plates (Analtech, Inc.; 1000 μm, 2000 μm, or 4000 μm). ^{1}H NMR spectra were recorded on a Bruker B-ACS-120 (400 MHz) spectrophotometer, a Varian Mercury (400 MHz) spectrophotometer, or a Varian VXR-300 (300 MHz) at room temperature. Chemical shifts are given in ppm (δ), coupling constants (*J*) are in hertz (Hz), and signals are designated as follows: (s) singlet, (d) doublet, (t) triplet, (q) quartet, (m) multiplet, (br s) broad singlet, (br d) broad doublet, (dd) doublet of doublet, (ddd) doublet of doublet of doublet. The purities of test compounds were determined by LCMS analysis, which was performed on a system consisting of an APCI ionization source on a Finnigan LCQ ion trap mass spectrometer, a Hewlett-Packard G1315A diode array detector, a Hewlett-Packard G1315A quaternary gradient pumping system, a Gilson 215 configured as an autosampler, and an Agilent Zorbax SB-C18 HPLC column (5 μm, 2.1 mm × 50 mm). The HPLC method incorporated UV detection at 214 nm, ambient column temperature, a flow rate of 1.0 mL/min, a 30 μL injection volume, and a binary solvent system of 0.01% TFA in water (solvent A) and 0.01% TFA in CH_3CN (solvent B). The following gradient (11 min) was used: 0−9 min, 5−100% B; 9−10 min, 100% B; 10−10.1 min, 5% B; 10.1−11 min, 5% B. All final compounds had a minimal purity of 98%, with the exception of **30** (95.7%). Elemental analyses of compounds evaluated in vivo were performed by QTI, Inc., Whitehouse, NJ, and were within ±0.4% of the theoretical values.

Syntheses of Phenoxybenzaldehydes (General Procedure A). The following procedure serves as a general method for the preparation of diaryl ether aldehydes.

3-Methoxy-4-(2-nitro-4-trifluoromethylphenoxy)benzaldehyde. A mixture of 2-fluoro-5-trifluoromethylnitrobenzene (640 mg, 3.06 mmol), vanillin (456 mg, 3 mmol), and K_2CO_3 (690 mg, 5 mmol) in DMF (3 mL) was heated at 95 °C for 5 h and then cooled to room temperature. Water (10 mL) was added, and the appropriate layer was extracted with EtOAc (3×), dried (Na_2SO_4), and concentrated. The residue was purified by silica gel chromatography [hexanes/ethyl acetate (4:1)] to afford the title benzaldehyde as slightly yellow-tinted white crystals. Yield: 950 mg (91%). ^{1}H NMR (400 MHz, $CDCl_3$) δ 10.00 (s, 1H), 8.29 (d, *J* = 2.35 Hz, 1H), 7.71 (dd, *J* = 1.96, 9.00 Hz, 1H), 7.58 (d, *J* = 1.96 Hz, 1H), 7.55 (dd, *J* = 1.76, 8.02 Hz, 1H), 7.29 (d, *J* = 7.83 Hz, 1H), 6.94 (d, *J* = 8.61 Hz, 1H), 3.87 (s, 3H).

Knoevenagel Condensations. The following procedures were used to condense the diaryl ether aldehydes of general procedure A with various carbon acids.

General Procedure B. Thiazolidine-2,4-dione (2.55 g, 21.79 mmol) and aldehyde from procedure A (21.79 mmol) were dissolved in toluene (150 mL) and treated with benzoic acid (3.27 mmol) and piperidine (2.83 mmol). The flask was equipped with a Dean−Stark trap, and the mixture was refluxed in a 130 °C oil bath for 12 h. After cooling to room temperature, the product was collected by filtration and triturated with hexanes to afford a pure product.

General Procedure C. Thiazolidine-2,4-dione (19 mg, 0.16 mmol), aldehyde from procedure A above (0.098 mmol), and NaOAc (30 mg, 0.37 mmol) were suspended in CH_3CN (2 mL) and heated to 105 °C (aluminum heating block). The CH_3CN was allowed to evaporate over 10−12 min and then repeated using two additional portions of CH_3CN (2 mL). The solid residue was cooled to room temperature. Then H_2O (2 mL) was added and the mixture heated to 75 °C for 10 min. The mixture was cooled to room temperature and the product was collected by filtration, dissolved in acetone, dried over Na_2SO_4, and concentrated under reduced pressure to afford the pure product.

General Procedure D. To a mixture of thiazolidine-2,4-dione (117 mg, 1.0 mmol) and aldehyde from procedure A (1.0 mmol) was added acetic acid (1.0 mL) and NH_4OAc (2.0 mmol). The suspension was heated at 100 °C (aluminum heating block) for 2−12 h. After the mixture was cooled to room temperature, the precipitated product was collected by filtration, washed with water, and triturated with EtOAc/hexanes to afford a pure product.

General Procedure E. A mixture of thiazolidine-2,4-dione (14.3 mg, 0.11 mmol), aldehyde from procedure A (0.1 mmol), NaOAc (25 mg, 0.3 mmol), and piperidine (1 drop) in EtOH (2 mL) and CH_3CN (4 mL) was heated at reflux overnight. The solvent was evaporated to a volume of ∼2 mL and cooled to room temperature. The precipitated product was collected by filtration and washed successively with CH_3CN and water to afford a pure product.

5-[3-Methoxy-4-(2-nitro-4-trifluoromethylphenoxy)benzylidene]-thiazolidine-2,4-dione (5). 3-Methoxy-4-(2-nitro-4-trifluoromethylphenoxy)benzaldehyde was condensed with 2,4-thiazolidinedione according to general procedure C to afford the title compound as a light-yellow powder (pale yellow needles from MeOH). Yield: 86%; mp: 203−204 °C. ^{1}H NMR (400 MHz, DMSO-d_6) δ 12.67 (br s, 1 H), 8.46 (d, *J* = 2.35 Hz, 1 H), 7.95 (dd, *J* = 8.80, 2.15 Hz, 1 H), 7.83 (s, 1 H), 7.50 (d, *J* = 1.96 Hz, 1 H), 7.43 (d, *J* = 8.22 Hz, 1 H), 7.28 (dd, *J* = 8.22, 1.96 Hz, 1 H), 7.08 (d, *J* = 9.00 Hz, 1 H), 3.80 (s, 3 H). MS (APCI+) *m*/*z* 439.8 [(M)$^{+\bullet}$]. MS (ESI+) *m*/*z* 463.2 (M + Na)$^+$, 504.3 (M + Na + AcCN)$^+$. t_R = 7.34 min (100%). Anal. Calcd for $C_{18}H_{11}F_3N_2O_6S$: C, 49.10%; H, 2.52%; N, 6.36%. Found: C, 49.18%; H, 2.45%; N, 6.45%.

4-[4-(2,4-Dioxothiazolidin-5-ylidenemethyl)-2-methoxyphenoxy]-2-trifluoromethylbenzonitrile (6). (A) 4-Fluoro-2-trifluoromethylbenzonitrile was reacted with vanillin according to general procedure A to afford 4-(4-formyl-2-methoxyphenoxy)-2-trifluoromethylbenzonitrile as a cream-colored granular solid. Yield: 97%. ^{1}H NMR (400 MHz, $CDCl_3$) δ 10.01 (s, 1H), 7.77 (d, *J* = 8.22 Hz, 1H), 7.60 (s, 1H), 7.57 (d, *J* = 9.00 Hz, 1H), 7.32 (d, *J* = 1.96 Hz, 1H), 7.28 (d, *J* = 8.22 Hz, 2H), 7.08 (dd, *J* = 2.15, 8.41 Hz, 1H), 3.87 (s, 3H).

(B) 4-(4-Formyl-2-methoxyphenoxy)-2-trifluoromethylbenzonitrile was condensed with 2,4-thiazolidinedione according to general procedure C to afford the title compound as an off-white powder. Yield: 81%. ^{1}H NMR (400 MHz, DMSO-d_6) δ 12.69 (br s, 1H), 8.10 (d, *J* = 8.61 Hz, 1H), 7.86 (s, 1H), 7.55 (d, *J* = 2.35 Hz, 1H), 7.52 (br s, 1H), 7.42 (d, *J* = 8.22 Hz, 1H), 7.28 (br d, *J* = 8.22 Hz, 1H), 7.22 (dd, *J* = 2.35, 8.61 Hz, 1H), 3.80 (s, 3H). MS (APCI+) *m*/*z* 419.9 [(M)$^{+\bullet}$]. t_R = 7.25 min (100%).

4-[4-(2,4-Dioxothiazolidin-5-ylidenemethyl)phenoxy]-2-trifluoromethylbenzonitrile (7). (A) 4-Fluoro-2-trifluoromethylbenzonitrile was reacted with 4-hydroxybenzaldehyde according to general procedure A to afford 4-(4-formylphenoxy)-2-trifluoromethylbenzonitrile as a pale yellow powder. Yield: 89%. ^{1}H NMR (400 MHz, $CDCl_3$) δ 10.01 (s, 1H), 7.98 (d, *J* = 7.04 Hz, 2H), 7.83 (d, *J* = 8.61 Hz, 1H), 7.42 (s, 1H), 7.02−7.36 (m, 3H).

(B) 4-(4-Formylphenoxy)-2-trifluoromethylbenzonitrile was condensed with 2,4-thiazolidinedione according to general procedure C to afford the title compound as a yellow powder. Yield: 88%. ^{1}H NMR (400 MHz, DMSO-d_6) δ 12.65 (br s, 1H), 8.18 (d, *J* = 8.61 Hz, 1H), 7.84 (s, 1H), 7.73 (d, *J* = 7.04 Hz, 2H), 7.68 (s, 1H), 7.45 (d, *J* = 8.61 Hz, 1H), 7.37 (d, *J* = 8.61 Hz, 2H). MS (APCI+) *m*/*z* 389.9 [(M)$^{+\bullet}$]. t_R = 7.22 min (98.3%).

4-[4-(2,4-Dioxothiazolidin-5-ylidenemethyl)-2-methylphenoxy]-2-trifluoromethylbenzonitrile (8). (A) 4-Fluoro-2-trifluoromethylbenzonitrile was reacted with 4-hydroxy-3-methylbenzaldehyde according to general procedure A to afford 4-(4-formyl-2-methylphenoxy)-2-trifluoromethylbenzonitrile as a light yellow solid. Yield: 86%. ^{1}H NMR (400 MHz, $CDCl_3$) δ 10.00 (s, 1H), 7.89 (s, 1H), 7.81 (d, J = 8.22 Hz, 2H), 7.36 (d, J = 2.35 Hz, 1H), 7.13 (dd, J = 2.35, 8.22 Hz, 1H), 7.11 (d, J = 8.22 Hz, 1H), 2.31 (s, 3H).

(B) 4-(4-Formyl-2-methylphenoxy)-2-trifluoromethylbenzonitrile was condensed with 2,4-thiazolidinedione according to general procedure C to afford the title compound as a yellowish-cream powder. Yield: 61%. ^{1}H NMR (300 MHz, DMSO-d_6) δ 12.66 (br s, 1H), 8.14 (d, J = 8.57 Hz, 1H), 7.79 (s, 1H), 7.63 (dd, J = 1.98, 8.90 Hz, 2H), 7.54 (dd, J = 1.98, 8.57 Hz, 1H), 7.23−7.34 (m, 2H), 2.21 (s, 3H). MS (APCI+) m/z 403.9 [$(M)^{+\bullet}$]. t_R = 7.53 min (99.6%).

4-[4-(2,4-Dioxothiazolidin-5-ylidenemethyl)-2-ethoxyphenoxy]-2-trifluoromethylbenzonitrile (9). (A) 4-Fluoro-2-trifluoromethylbenzonitrile was reacted with 3-ethoxy-4-hydroxybenzaldehyde according to general procedure A to afford 4-(4-formyl-2-ethoxyphenoxy)-2-trifluoromethylbenzonitrile as a cream-colored solid. Yield: 97%. ^{1}H NMR (400 MHz, $CDCl_3$) δ 9.99 (s, 1H), 7.76 (d, J = 8.61 Hz, 1H), 7.52−7.57 (m, 2H), 7.31 (d, J = 2.74 Hz, 1H), 7.29 (d, J = 7.83 Hz, 1H), 7.10 (dd, J = 2.74, 8.61 Hz, 1H), 4.10 (q, J = 7.04 Hz, 2H), 1.23 (t, J = 6.85 Hz, 3H).

(B) 4-(4-Formyl-2-ethoxyphenoxy)-2-trifluoromethylbenzonitrile was condensed with 2,4-thiazolidinedione according to general procedure C to afford the title compound as a slightly yellow-tinted white solid. Yield: 59%. ^{1}H NMR (400 MHz, DMSO-d_6) δ 12.66 (br s, 1H), 8.09 (d, J = 8.61 Hz, 1H), 7.83 (s, 1H), 7.51 (d, J = 2.74 Hz, 1H), 7.46 (d, J = 1.96 Hz, 1H), 7.41 (d, J = 8.61 Hz, 1H), 7.25 (ddd, J = 2.54, 2.74, 8.41 Hz, 3H), 4.07 (q, J = 6.78 Hz, 3H). MS (APCI+) m/z 434.0 [$(M)^{+\bullet}$]. t_R = 7.58 min (100%).

4-[4-(2,4-Dioxothiazolidin-5-ylidenemethyl)-3-methoxyphenoxy]-2-trifluoromethylbenzonitrile (10). (A) 4-Fluoro-2-trifluoromethylbenzonitrile was reacted with 4-hydroxy-2-methoxybenzaldehyde according to general procedure A to afford 4-(4-formyl-3-methoxyphenoxy)-2-trifluoromethylbenzonitrile as an off-white solid. Yield: 95%. ^{1}H NMR (400 MHz, $CDCl_3$) δ 10.42 (s, 1H), 7.92 (d, J = 8.61 Hz, 1H), 7.84 (d, J = 8.61 Hz, 1H), 7.44 (d, J = 2.35 Hz, 1H), 7.28−7.24 (m, 1H), 6.71 (d, J = 1.96 Hz, 1H), 6.68 (br d, J = 8.22 Hz, 1H), 3.93 (s, 3H).

(B) 4-(4-Formyl-3-methoxyphenoxy)-2-trifluoromethylbenzonitrile was condensed with 2,4-thiazolidinedione according to general procedure C to afford the title compound as a canary-yellow powder. Yield: 87%. ^{1}H NMR (400 MHz, DMSO-d_6) δ 12.59 (br s, 1H), 8.16 (d, J = 8.61 Hz, 1H), 7.92 (s, 1H), 7.68 (d, J = 2.35 Hz, 1H), 7.49 (d, J = 8.22 Hz, 1H), 7.45 (dd, J = 2.74, 8.61 Hz, 1H), 7.05 (d, J = 2.35 Hz, 1H), 6.89 (dd, J = 2.15, 8.41 Hz, 1H), 3.87 (s, 3H). MS (APCI+) m/z 420.0 [$(M)^{+\bullet}$]. t_R = 7.35 min (99.4%).

4-[4-(2,4-Dioxothiazolidin-5-ylidenemethyl)-2,6-dimethoxyphenoxy]-2-trifluoromethylbenzonitrile (11). (A) 4-Fluoro-2-trifluoromethylbenzonitrile was reacted with 3,5-dimethoxy-4-hydroxybenzaldehyde according to general procedure A to afford 4-(4-formyl-2,6-dimethoxyphenoxy)-2-trifluoromethylbenzonitrile as an off-white solid. Yield: 50%. ^{1}H NMR (400 MHz, $CDCl_3$) δ 9.97 (s, 1H), 7.72 (d, J = 8.61 Hz, 1H), 7.28 (d, J = 2.35 Hz, 1H), 7.23 (s, 2H), 7.00 (dd, J = 2.54, 8.41 Hz, 1H), 3.88 (s, 6H).

(B) 4-(4-Formyl-2,6-dimethoxyphenoxy)-2-trifluoromethylbenzonitrile was condensed with 2,4-thiazolidinedione according to general procedure C to afford the title compound as an off-white powder. Yield: 67%. ^{1}H NMR (400 MHz, DMSO-d_6) δ 12.70 (br s, 1H), 8.05 (d, J = 9.00 Hz, 1H), 7.83 (s, 1H), 7.50 (d, J = 2.35 Hz, 1H), 7.13 (dd, J = 2.35, 8.61 Hz, 1H), 7.08 (s, 2H), 3.79 (s, 6H). MS (APCI+) m/z 449.9 [$(M)^{+\bullet}$]. t_R = 7.19 min (100%).

4-[4-(2,4-Dioxothiazolidin-5-ylidenemethyl)naphthalen-1-yloxy]-2-trifluoromethylbenzonitrile (12). (A) 4-Fluoro-2-trifluoromethylbenzonitrile was reacted with 4-hydroxynaphthaldehyde according to general procedure A to afford 4-(4-formylnaphthalen-1-yloxy)-2-trifluoromethylbenzonitrile as a tan-colored solid. Yield: 76%. ^{1}H NMR (400 MHz, $CDCl_3$) δ 10.36 (s, 1H), 9.37 (d, J = 8.61 Hz, 1H), 8.16 (d, J = 8.61 Hz, 1H), 8.01 (d, J = 7.83 Hz, 1H), 7.84 (d, J = 8.61 Hz, 1H), 7.80 (t, J = 7.83 Hz, 1H), 7.66 (t, J = 7.66 Hz, 1H), 7.53 (d, J = 2.35 Hz, 1H), 7.26 (dd, J = 8.22, 2.35 Hz, 1H), 7.15 (d, J = 7.83 Hz, 1H).

(B) 4-(4-Formylnaphthalen-1-yloxy)-2-trifluoromethylbenzonitrile was condensed with 2,4-thiazolidinedione according to general procedure C to afford the title compound as fine bright yellow crystals (from acetone/hexane). Yield: 22%. ^{1}H NMR (300 MHz, acetone-d_6) δ 11.19 (br s, 1H), 8.50 (s, 1H), 8.31 (d, J = 8.57 Hz, 1H), 8.20 (d, J = 8.57 Hz, 1H), 8.11 (d, J = 8.57 Hz, 1H), 7.66−7.87 (m, 4H), 7.49 (dd, J = 2.97, 8.57 Hz, 1H), 7.46 (d, J = 7.91 Hz, 1H). MS (APCI+) m/z 439.9 [$(M)^{+\bullet}$]. t_R = 7.84 min (98.6%).

5-[3-Methoxy-4-(2-nitrophenoxy)benzylidene]thiazolidine-2,4-dione (13). (A) 2-Nitrofluorobenzene was reacted with vanillin according to general procedure A to afford 3-methoxy-4-(2-nitrophenoxy)benzaldehyde as a yellow granular solid. Yield: 86%. ^{1}H NMR (400 MHz, $CDCl_3$) δ 9.94 (s, 1H), 8.03 (dd, J = 1.96, 8.22 Hz, 1H), 7.50−7.58 (m, 2H), 7.46 (dd, J = 1.96, 8.22 Hz, 1H), 7.24−7.31 (m, 1H), 7.06 (d, J = 8.22 Hz, 1H), 7.00 (dd, J = 1.17, 8.61 Hz, 1H), 3.91 (s, 3H).

(B) 3-Methoxy-4-(2-nitrophenoxy)benzaldehyde was condensed with 2,4-thiazolidinedione according to general procedure D to afford the title compound as small pale orange-yellow crystals. Yield: 88%. ^{1}H NMR (400 MHz, DMSO-d_6) δ 12.66 (br s, 1H), 8.06 (dd, J = 1.56, 8.22 Hz, 1H), 7.84 (s, 1H), 7.64 (ddd, J = 1.76, 7.24, 8.61 Hz, 1H), 7.47 (d, J = 1.57 Hz, 1H), 7.29−7.35 (m, 1H), 7.20−7.27 (m, 2H), 6.98 (dd, J = 1.17, 8.22 Hz, 1H), 3.81 (s, 3H). MS (APCI+) m/z 371.7 [$(M)^{+\bullet}$] (minor; poor ionization). MS (ESI+) m/z 373.2 $(M + H)^+$, 395.2 $(M + Na)^+$, 436.2 $(M + Na + AcCN)^+$. t_R = 6.54 min (100%).

4-[4-(2,4-Dioxothiazolidin-5-ylidenemethyl)-2-methoxyphenoxy]-3-nitrobenzoic Acid Methyl Ester (14). + (A) Methyl 4-fluoro-3-nitrobenzoate was reacted with vanillin according to general procedure A to afford 4-(4-formyl-2-methoxyphenoxy)-3-nitrobenzoic acid methyl ester as a pale yellow solid. Yield: 75%. ^{1}H NMR (400 MHz, $CDCl_3$) δ 9.98 (s, 1H), 8.65 (d, J = 2.35 Hz, 1H), 8.13 (dd, J = 1.96, 8.61 Hz, 1H), 7.56−7.58 (m, J = 1.96 Hz, 1H), 7.54 (dd, J = 1.57, 8.22 Hz, 1H), 7.28 (d, J = 7.83 Hz, 1H), 6.88 (d, J = 9.00 Hz, 1H), 3.96 (s, 3H), 3.86 (s, 3H).

(B) 4-(4-Formyl-2-methoxyphenoxy)-3-nitrobenzoic acid methyl ester was condensed with 2,4-thiazolidinedione according to general procedure D to afford the title compound as a fluffy pale yellow powder. Yield: 91%. ^{1}H NMR (400 MHz, DMSO-d_6) δ 12.69 (br s, 1H), 8.53 (d, J = 2.35 Hz, 1H), 8.12 (dd, J = 2.15, 8.80 Hz, 1H), 7.86 (s, 1H), 7.52 (d, J = 1.96 Hz, 1H), 7.44 (d, J = 8.61 Hz, 1H), 7.28 (dd, J = 1.96, 8.22 Hz, 1H), 7.00 (d, J = 8.61 Hz, 1H), 3.88 (s, 3H), 3.79 (s, 3H). MS (APCI+) m/z 429.8 [$(M)^{+\bullet}$]. t_R = 6.80 min (100%).

4-[4-(2,4-Dioxothiazolidin-5-ylidenemethyl)-2-methoxyphenoxy]-3-nitrobenzonitrile (15). + (A) 4-Fluoro-3-nitrobenzonitrile was reacted with vanillin according to general procedure A to afford 4-(4-formyl-2-methoxyphenoxy)-3-nitrobenzonitrile as a light yellow powder. Yield: 97%. ^{1}H NMR (400 MHz, $CDCl_3$) δ 10.00 (s, 1H), 8.31 (d, J = 1.96 Hz, 1H), 7.71 (dd, J = 2.15, 8.80 Hz, 1H), 7.53−7.60 (m, 2H), 7.34 (d, J = 8.61 Hz, 1H), 6.88 (d, J = 9.00 Hz, 1H), 3.85 (s, 3H).

(B) 4-(4-Formyl-2-methoxyphenoxy)-3-nitrobenzonitrile was condensed with 2,4-thiazolidinedione according to general procedure C to afford the title compound as a yellow powder. Yield: 73%. ^{1}H NMR (400 MHz, DMSO-d_6) δ 12.67 (br s, 1H), 8.66 (d, J = 1.96 Hz, 1H), 8.03 (dd, J = 1.96, 8.61 Hz, 1H), 7.85 (s, 1H), 7.51 (d, J = 1.96 Hz, 1H), 7.43 (d, J = 8.22 Hz, 1H), 7.28 (dd, J = 1.76, 8.41 Hz, 1H), 7.04 (d, J = 9.00 Hz, 1H), 3.79 (s, 3H). MS (APCI+) m/z 396.7 [$(M)^{+\bullet}$]. t_R = 6.54 min (98.3%).

5-[3-Methoxy-4-(4-nitro-3-trifluoromethylphenoxy)benzylidene]-thiazolidine-2,4-dione (16). (A) 5-Fluoro-2-nitrobenzotrifluoride was reacted with vanillin according to general procedure A to afford methyl 3-methoxy-4-(4-nitro-3-trifluoromethylphenoxy)-benzaldehyde as a pale yellow solid. Yield: 98%. ^{1}H NMR (400 MHz, $CDCl_3$) δ 10.01 (s, 1H), 7.96 (d, J = 9.00 Hz, 1H), 7.60 (d, J = 1.57 Hz, 1H), 7.57 (dd, J = 1.76, 8.02 Hz, 1H), 7.35 (d, J = 2.74 Hz, 1H), 7.29 (d, J = 8.22 Hz, 1H), 7.07 (dd, J = 2.74, 9.00 Hz, 1H), 3.88 (s, 3H).

(B) 3-Methoxy-4-(4-nitro-3-trifluoromethylphenoxy)benzaldehyde was condensed with 2,4-thiazolidinedione according to general procedure D to afford the title compound as a very pale yellow-tinted powder. Yield: 84%. ^{1}H NMR (400 MHz, DMSO-d_6) δ 12.70 (br s, 1H), 8.17 (d, J = 9.00 Hz, 1H), 7.87 (s, 1H), 7.58 (d, J = 2.74 Hz, 1H), 7.53 (d, J = 1.96 Hz, 1H), 7.44 (d, J = 8.61 Hz, 1H), 7.29 (dd, J = 1.96, 8.22 Hz, 1H), 7.24 (dd, J = 2.74, 9.00 Hz, 1H), 3.81 (s, 3H). MS (APCI+) m/z 439.9 [$(M)^{+\bullet}$]. t_R = 7.45 min (100%).

2-[4-(2,4-Dioxothiazolidin-5-ylidenemethyl)-2-methoxyphenoxy]-5-nitrobenzonitrile (17). (A) 2-Fluoro-5-nitrobenzonitrile was reacted with vanillin according to general procedure A to afford 2-(4-formyl-2-methoxyphenoxy)-5-nitrobenzonitrile as a fluffy tan-colored solid. Yield: 80%. ^{1}H NMR (400 MHz, $CDCl_3$) δ 10.02 (s, 1H), 8.58 (d, J = 2.74 Hz, 1H), 8.30 (dd, J = 2.74, 9.00 Hz, 1H), 7.57−7.61 (m, 2H), 7.39 (d, J = 8.22 Hz, 1H), 7.23−7.28 (m, 1H), 6.75 (d, J = 9.00 Hz, 1H), 3.85 (s, 3H).

(B) 2-(4-Formyl-2-methoxyphenoxy)-5-nitrobenzonitrile was condensed with 2,4-thiazolidinedione according to general procedure C to afford the title compound as a pale yellow powder. Yield: 86%. ^{1}H NMR (400 MHz, DMSO-d_6) δ 12.67 (br s, 1H), 8.84 (d, J = 2.74 Hz, 1H), 8.38 (dd, J = 3.13, 9.39 Hz, 1H), 7.85 (s, 1H), 7.53 (d, J = 1.57 Hz, 1H), 7.51 (d, J = 8.61 Hz, 1H), 7.30 (dd, J = 1.76, 8.41 Hz, 1H), 6.92 (d, J = 9.39 Hz, 1H), 3.80 (s, 3H). MS (APCI+) m/z 396.9 [$(M)^{+\bullet}$]. t_R = 6.66 min (99.0%).

2-[4-(2,4-Dioxothiazolidin-5-ylidenemethyl)-2-methoxyphenoxy]-benzonitrile (18). (A) 2-Fluorobenzonitrile was reacted with vanillin according to general procedure A to afford 2-(4-formyl-2-methoxyphenoxy)benzonitrile as an opaque syrup that solidified on standing. Yield: 83%. ^{1}H NMR (400 MHz, $CDCl_3$) δ 9.97 (s, 1H), 7.68 (dd, J = 1.56, 7.83 Hz, 1H), 7.56 (d, J = 1.57 Hz, 1H), 7.45−7.52 (m, 2H), 7.14−7.21 (m, 2H), 6.79 (d, J = 8.22 Hz, 1H), 3.88 (s, 3H).

(B) 2-(4-Formyl-2-methoxyphenoxy)benzonitrile was condensed with 2,4-thiazolidinedione according to general procedure D to afford the title compound as a pale yellow powder. Yield: 84%. ^{1}H NMR (400 MHz, DMSO-d_6) δ 12.68 (br s, 1H), 7.88 (dd, J = 1.57, 7.83 Hz, 1H), 7.86 (s, 1H), 7.61 (ddd, J = 1.76, 7.24, 8.61 Hz, 1H), 7.49 (d, J = 1.96 Hz, 1H), 7.35 (d, J = 8.22 Hz, 1H), 7.21−7.29 (m, 2H), 6.79 (d, J = 8.22 Hz, 1H), 3.81 (s, 3H). MS (APCI+) m/z 353.1 $(M + H)^+$. t_R = 6.43 min (100%).

4-[4-(2,4-Dioxothiazolidin-5-ylidenemethyl)-2-methoxyphenoxy]-isophthalonitrile (19). (A) 4-Fluoroisophthalonitrile was reacted with vanillin according to general procedure A to afford 4-(4-formyl-2-methoxyphenoxy)isophthalonitrile as a pale yellowish cream-colored powder. Yield: 100%. ^{1}H NMR (400 MHz, $CDCl_3$) δ 10.01 (s, 1H), 7.98 (d, J = 1.96 Hz, 1H), 7.70 (dd, J = 2.15, 8.80 Hz, 1H), 7.61−7.55 (m, 2H), 7.36−7.35 (m, 1H), 6.73 (d, J = 9.00 Hz, 1H), 3.85 (s, 3H).

(B) 4-(4-Formyl-2-methoxyphenoxy)isophthalonitrile was condensed with 2,4-thiazolidinedione according to general procedure D to afford the title compound as a light beige-colored solid. Yield: 99%. ^{1}H NMR (400 MHz, DMSO-d_6) δ 12.70 (br s, 1H), 8.55 (d, J = 1.96 Hz, 1H), 8.03 (dd, J = 1.96, 9.00 Hz, 1H), 7.87 (s, 1H), 7.53 (d, J = 2.35 Hz, 1H), 7.49 (d, J = 8.22 Hz, 1H), 7.30 (dd, J = 1.96, 8.22 Hz, 1H), 6.89 (d, J = 9.00 Hz, 1H), 3.80 (s, 3H). MS (APCI+) m/z 377.0 [$(M)^{+\bullet}$]. t_R = 6.39 min (100%).

2-[4-(2,4-Dioxothiazolidin-5-ylidenemethyl)-2-methoxyphenoxy]-5-trifluoromethylbenzonitrile (20). (A) 2-Fluoro-5-trifluoromethylbenzonitrile was reacted with vanillin according to general procedure A to afford 2-(4-formyl-2-methoxyphenoxy)-5-trifluoromethylbenzonitrile as a pale yellow oil that solidified over several days. Yield: 94%. ^{1}H NMR (400 MHz, $CDCl_3$) δ 10.00 (s, 1H), 7.94 (d, J = 2.35 Hz, 1H), 7.68 (dd, J = 1.96, 8.61 Hz, 1H), 7.54−7.60 (m, 2H), 7.33 (d, J = 7.83 Hz, 1H), 6.77 (d, J = 9.00 Hz, 1H), 3.86 (s, 3H).

(B) 2-(4-Formyl-2-methoxyphenoxy)-5-trifluoromethylbenzonitrile was condensed with 2,4-thiazolidinedione according to general procedure D to afford the title compound as a pale yellowish cream-colored powder. Yield: 77%. ^{1}H NMR (400 MHz, $CDCl_3$) δ ^{1}H NMR (400 MHz, DMSO-d_6) δ 12.70 (br s, 1H), 8.43 (d, J = 1.96 Hz, 1H), 7.94 (dd, J = 2.15, 9.19 Hz, 1H), 7.87 (s, 1H), 7.53 (d, J = 1.96 Hz, 1H), 7.49 (d, J = 8.61 Hz, 1H), 7.30 (dd, J = 1.96, 8.22 Hz, 1H), 6.92 (d, J = 9.00 Hz, 1H), 3.81 (s, 3H). MS (APCI+) m/z 420.0 [$(M)^{+\bullet}$]. t_R = 7.23 min (100%).

4-[4-(2,4-Dioxothiazolidin-5-ylidenemethyl)-2-methoxyphenoxy]-3-chlorobenzoic Acid Methyl Ester (21). + (A) Methyl 4-fluoro-3-chlorobenzoate was reacted with vanillin according to general procedure A to afford 4-(4-formyl-2-methoxyphenoxy)-3-chlorobenzoic acid methyl ester as a colorless syrup. Yield: 97%. ^{1}H NMR (400 MHz, $CDCl_3$) δ 9.95 (s, 1H), 8.17 (d, J = 2.35 Hz, 1H), 7.88 (dd, J = 2.35, 8.61 Hz, 1H), 7.56 (d, J = 1.57 Hz, 1H), 7.47 (dd, J = 1.76, 8.02 Hz, 1H), 7.04 (d, J = 7.83 Hz, 1H), 6.86 (d, J = 8.22 Hz, 1H), 3.93 (s, 3H), 3.92 (s, 7H).

(B) 4-(4-Formyl-2-methoxyphenoxy)-3-chlorobenzoic acid methyl ester was condensed with 2,4-thiazolidinedione according to general procedure D to afford the title compound as a pale canary-yellow powder. Yield: 80%. ^{1}H NMR (400 MHz, DMSO-d_6) δ 12.68 (br s, 1H), 8.06 (d, J = 2.35 Hz, 1H), 7.85 (s, 1H), 7.84 (dd, J = 1.96, 8.61 Hz, 1H), 7.50 (d, J = 1.96 Hz, 1H), 7.31 (d, J = 8.22 Hz, 1H), 7.26 (dd, J = 1.96, 8.22 Hz, 1H), 6.83 (d, J = 8.61 Hz, 1H), 3.85 (s, 3H), 3.80 (s, 3H). MS (APCI+) m/z 418.9 [$(M)^{+\bullet}$]. t_R = 7.29 min (100%).

5-[4-(2-Chloro-4-trifluoromethylphenoxy)-3-methoxybenzylidene]thiazolidine-2,4-dione (22). (A) 3-Chloro-4-fluorobenzotrifluoride was reacted with vanillin according to general procedure A to afford 4-(2-chloro-4-trifluoromethylphenoxy)-3-methoxybenzaldehyde as a colorless oil. Yield: 64%. ^{1}H NMR (400 MHz, $CDCl_3$) δ 9.95 (s, 1H), 7.75 (d, J = 2.02 Hz, 1H), 7.57 (d, J = 1.77 Hz, 1H), 7.43−7.50 (m, 2H), 7.04 (d, J = 8.08 Hz, 1H), 6.92 (d, J = 8.59 Hz, 1H), 3.92 (s, 3H).

(B) 4-(2-Chloro-4-trifluoromethylphenoxy)-3-methoxybenzaldehyde was condensed with 2,4-thiazolidinedione according to general procedure D to afford the title compound as a fluffy, slightly yellow-tinted white solid. Yield: 86%. ^{1}H NMR (400 MHz, DMSO-d_6) δ 12.68 (br s, 1H), 8.02 (d, J = 1.96 Hz, 1H), 7.85 (s, 1H), 7.64 (dd, J = 1.96, 8.61 Hz, 1H), 7.50 (d, J = 1.96 Hz, 1H), 7.31 (d, J = 8.22 Hz, 1H), 7.25 (dd, J = 1.96, 8.22 Hz, 1H), 6.91 (d, J = 8.61 Hz, 1H), 3.82 (s, 3H). MS (APCI+) m/z 428.9 [$(M)^{+\bullet}$]. t_R = 7.95 min (100%).

4-[4-(2,4-Dioxothiazolidin-5-ylidenemethyl)-2-methoxyphenoxy]-3-chlorobenzonitrile (23). (A) 3-Chloro-4-fluorobenzonitrile was reacted with vanillin according to general procedure A to afford 4-(4-formyl-2-methoxyphenoxy)-3-chlorobenzonitrile as a cream-colored solid. Yield: 89%. ^{1}H NMR (400 MHz, $CDCl_3$) δ 9.96 (s, 1H), 7.76 (s, 1H), 7.56 (s, 1H), 7.50 (d, J = 7.83 Hz, 1H), 7.45 (d, J = 8.61 Hz, 1H), 7.15 (d, J = 8.22 Hz, 1H), 6.77 (d, J = 8.22 Hz, 1H), 3.87 (s, 3H).

(B) 4-(4-Formyl-2-methoxyphenoxy)-3-chlorobenzonitrile was condensed with 2,4-thiazolidinedione according to general procedure C to afford the title compound as a bright yellow powder. Yield: 78%. ^{1}H NMR (400 MHz, DMSO-d_6) δ 12.64 (br s, 1H), 8.17 (d, J = 1.96 Hz, 1H), 7.83 (s, 1H), 7.71 (dd, J = 2.15, 8.80 Hz, 1H), 7.47 (d, J = 1.96 Hz, 1H), 7.31 (d, J = 8.22 Hz, 1H), 7.24 (dd, J = 1.96, 8.22 Hz, 1H), 6.83 (d, J = 8.61 Hz, 1H), 3.78 (s, 3H). MS (APCI+) m/z 385.9 [$(M)^{+\bullet}$]. t_R = 7.05 min (100%).

4-[4-(2,4-Dioxothiazolidin-5-ylidenemethyl)-2-methoxyphenoxy]-3-bromobenzoic Acid Methyl Ester (24). (A) Methyl 4-fluoro-3-bromobenzoate was reacted with vanillin according to general procedure A to afford 4-(4-formyl-2-methoxyphenoxy)-3-bromobenzoic acid methyl ester as a colorless syrup. Yield: 79%. ^{1}H

NMR (400 MHz, $CDCl_3$) δ 9.93 (s, 1H), 8.31 (br s, 1H), 7.89 (br d, J = 8.61 Hz, 1H), 7.54 (s, 1H), 7.45 (br d, J = 8.22 Hz, 1H), 7.04 (d, J = 7.83 Hz, 1H), 6.79 (d, J = 8.61 Hz, 1H), 3.90 (s, 3H), 3.89 (s, 3H).

(B) 4-(4-Formyl-2-methoxyphenoxy)-3-bromobenzoic acid methyl ester was condensed with 2,4-thiazolidinedione according to general procedure C to afford the title compound as an off-white solid. Yield: 82%. ^{1}H NMR (400 MHz, DMSO-d_6) δ 8.17 (d, J = 1.96 Hz, 1H), 7.85 (dd, J = 1.96, 8.61 Hz, 1H), 7.71 (s, 1H), 7.44 (d, J = 1.57 Hz, 1H), 7.25 (d, J = 8.61 Hz, 1H), 7.22 (dd, J = 1.57, 8.61 Hz, 1H), 6.77 (d, J = 8.61 Hz, 1H), 3.82 (s, 3H), 3.78 (s, 3H). MS (APCI+) m/z 462.8 [$(M)^{+\bullet}$]. t_R = 7.41 min (99.4%).

5-[4-(2-Bromo-4-trifluoromethylphenoxy)-3-methoxybenzylidene]thiazolidine-2,4-dione (25). (A) 3-Bromo-4-fluorobenzotri + fluoride was reacted with vanillin according to general procedure A (reaction temperature was 150 °C, 5 h) to afford 4-(2-bromo-4-trifluoromethylphenoxy)-3-methoxybenzaldehyde as an opaque syrup. Yield: 65%. ^{1}H NMR (400 MHz, $CDCl_3$) δ 9.96 (s, 1H), 7.92 (d, J = 1.96 Hz, 1H), 7.57 (d, J = 1.57 Hz, 1H), 7.45−7.53 (m, 2H), 7.06 (d, J = 8.22 Hz, 1H), 6.87 (d, J = 8.61 Hz, 1H), 3.92 (s, 3H).

(B) 4-(2-Bromo-4-trifluoromethylphenoxy)-3-methoxybenzaldehyde was condensed with 2,4-thiazolidinedione according to general procedure C to afford the title compound as a pale yellow powder. Yield: 87%. ^{1}H NMR (400 MHz, DMSO-d_6) δ 12.64 (br s, 1H), 8.09 (d, J = 1.96 Hz, 1H), 7.73 (s, 1H), 7.65 (dd, J = 1.96, 8.61 Hz, 1H), 7.46 (d, 1H), 7.25 (d, J = 8.22 Hz, 1H), 7.23 (dd, J = 1.57, 8.22 Hz, 1H), 6.85 (d, J = 8.61 Hz, 1H), 3.80 (s, 3H). MS (APCI+) m/z 472.8 [$(M)^{+\bullet}$]. t_R = 8.03 min (100%).

4-[4-(2,4-Dioxothiazolidin-5-ylidenemethyl)-2-methoxyphenoxy]-3-bromobenzonitrile (26). (A) 3-Bromo-4-fluorobenzonitrile was reacted with vanillin according to general procedure A to afford 4-(4-formyl-2-methoxyphenoxy)-3-bromobenzonitrile as an off-white powder. Yield: 73%. ^{1}H NMR (400 MHz, $CDCl_3$) δ 9.96 (s, 1H), 7.92 (d, J = 1.56 Hz, 1H), 7.55 (s, 1H), 7.43−7.54 (m, 2H), 7.16 (d, J = 8.22 Hz, 1H), 6.73 (d, J = 8.61 Hz, 1H), 3.87 (s, 3H).

(B) 4-(4-Formyl-2-methoxyphenoxy)-3-bromobenzonitrile was condensed with 2,4-thiazolidinedione according to general procedure C to afford the title compound as a yellow powder. Yield: 94%. ^{1}H NMR (400 MHz, DMSO-d_6) δ 12.63 (br s, 1H), 8.28 (d, J = 1.96 Hz, 1H), 7.83 (s, 1H), 7.74 (dd, J = 1.96, 8.61 Hz, 1H), 7.47 (d, J = 1.57 Hz, 1H), 7.29 (d, J = 8.61 Hz, 1H), 7.24 (dd, J = 1.96, 8.22 Hz, 1H), 6.79 (d, J = 8.61 Hz, 1H), 3.78 (s, 3H). MS (APCI+) m/z 429.9 [$(M)^{+\bullet}$]. t_R = 7.11 min (100%).

4-[4-(2,4-Dioxothiazolidin-5-ylidenemethyl)-2-methoxyphenoxy]-3-trifluoromethylbenzoic Acid Methyl Ester (27). (A) 4-Fluoro-3-trifluoromethylbenzoic acid methyl ester was reacted with vanillin according to general procedure A to afford 4-(4-formyl-2-methoxy-phenoxy)-3-trifluoromethylbenzoic acid methyl ester as a pale yellow oil that solidified after several days. Yield: 54%. ^{1}H NMR (400 MHz, $CDCl_3$) δ 9.98 (s, 1H), 8.38 (d, J = 1.96 Hz, 1H), 8.09 (dd, J = 1.96, 8.61 Hz, 1H), 7.56 (d, J = 1.96 Hz, 1H), 7.52 (dd, J = 1.76, 8.02 Hz, 1H), 7.23 (d, J = 7.83 Hz, 1H), 6.76 (d, J = 8.61 Hz, 1H), 3.94 (s, 3H), 3.85 (s, 3H).

(B) 4-(4-Formyl-2-methoxyphenoxy)-3-trifluoromethylbenzoic acid methyl ester was condensed with 2,4-thiazolidinedione according to general procedure D to afford the title compound as an off-white solid. Yield: 78%. ^{1}H NMR (400 MHz, $CDCl_3$) δ ^{1}H NMR (400 MHz, DMSO-d_6) δ 12.69 (br s, 1H), 8.22 (d, J = 1.96 Hz, 1H), 8.13 (dd, J = 2.15, 8.80 Hz, 1H), 7.86 (s, 1H), 7.52 (d, J = 1.96 Hz, 1H), 7.38 (d, J = 8.22 Hz, 1H), 7.28 (dd, J = 1.96, 8.61 Hz, 1H), 6.90 (d, J = 9.00 Hz, 1H), 3.87 (s, 3H), 3.79 (s, 3H). MS (APCI+) m/z 452.9 [$(M)^{+\bullet}$]. t_R = v 7.50 min (100%).

5-[4-(2,4-Bis-trifluoromethylphenoxy)-3-methoxybenzylidene]-thiazolidine-2,4-dione (28). (A) 1-Fluoro-2,4-bis-trifluoromethylbenzene was reacted with vanillin according to general procedure A to afford 4-(2,4-bis-trifluoromethylphenoxy)-3-methoxybenzaldehyde as a colorless syrup. Yield: 87%. ^{1}H NMR (400 MHz, $CDCl_3$) δ 9.99 (s, 1H), 7.95 (d, J = 1.56 Hz, 1H), 7.67 (dd, J = 2.15, 8.80 Hz, 1H), 7.58 (d, J = 1.96 Hz, 1H), 7.53 (dd, J = 1.76, 8.02 Hz, 1H), 7.24 (d, J = 7.83 Hz, 1H), 6.81 (d, J = 8.61 Hz, 1H), 3.87 (s, 3H).

(B) 4-(2,4-Bis-trifluoromethylphenoxy)-3-methoxybenzaldehyde was condensed with 2,4-thiazolidinedione according to general procedure D to afford the title compound as cream-colored granules (from MeOH). Yield: 72%. ^{1}H NMR (400 MHz, DMSO-d_6) δ 12.69 (br s, 1H), 8.07 (d, J = 1.96 Hz, 1H), 7.95 (dd, J = 2.15, 8.80 Hz, 1H), 7.87 (s, 1H), 7.52 (d, J = 1.96 Hz, 1H), 7.35−7.40 (m, 1H), 7.28 (dd, J = 1.96, 8.22 Hz, 1H), 6.97 (d, J = 8.61 Hz, 1H), 3.80 (s, 3H). MS (APCI+) m/z 463.0 [$(M)^{+\bullet}$]. t_R = 8.06 min (98.6%).

4-[4-(2,4-Dioxothiazolidin-5-ylidenemethyl)-2-methoxyphenoxy]-3-trifluoromethylbenzonitrile (29). (A) 4-Fluoro-3-trifluoromethylbenzonitrile was reacted with vanillin according to general procedure A to afford 4-(4-formyl-2-methoxyphenoxy)-3-trifluoromethylbenzonitrile as a white solid. Yield: 71%. ^{1}H NMR (400 MHz, $CDCl_3$) δ 10.41 (s, 1H), 7.91 (d, J = 8.61 Hz, 1H), 7.83 (d, J = 8.61 Hz, 1H), 7.43 (d, J = 2.35 Hz, 1H), 7.25 (dd, J = 2.35, 9.00 Hz, 1H), 6.70 (d, J = v 2.35 Hz, 1H), 6.67 (d, J = 8.22 Hz, 1H), 3.92 (s, 3H).

(B) 4-(4-Formyl-2-methoxyphenoxy)-3-trifluoromethylbenzonitrile was condensed with 2,4-thiazolidinedione according to the procedure B to afford the title compound as a pale yellow solid. Yield: 84%. Mp: 205.2 °C. ^{1}H NMR (400 MHz, DMSO-d_6) δ 12.67 (br s, 1H), 8.31 (d, J = 1.96 Hz, 1H), 8.00 (dd, J = 2.15, 8.80 Hz, 1H), 7.84 (s, 1H), 7.49 (d, J = 1.96 Hz, 1H), 7.36 (d, J = 8.22 Hz, 1H), 7.26 (dd, J = 1.96, 8.61 Hz, 1H), 6.90 (d, J = 9.00 Hz, 1H), 3.77 (s, 3H). MS (APCI+) m/z 419.9 [$(M)^{+\bullet}$]. t_R = 7.19 min (100%). Anal. Calcd for $C_{19}H_{11}F_3N_2O_4S$: C, 54.29%; H, 2.64%; N, 6.66%. Found: C, 54.49%; H, 2.29%; N, 6.67%.

5-[4-(2-Trifluoromethylphenoxy)-3-methoxybenzylidene]-thiazolidine-2,4-dione (30). (A) A mixture of 2-fluorobenzotrifluoride (0.5 mL), vanillin (152 mg, 1 mmol), and dimethylacetamide (1.5 mL) was heated to 220 °C in a microwave reactor for 0.5 h. The mixture was then partitioned between water and EtOAc, and the organic phase was concentrated. The residue was purified by radial chromatography [hexane/EtOAc (8:1)] to afford 4-(2-trifluoromethylphenoxy)-3-methoxybenzaldehyde as a colorless oil. Yield: 9%. ^{1}H NMR (400 MHz, $CDCl_3$) δ 9.94 (s, 1H), 7.71 (dd, J = 7.83, 1.17 Hz, 1H), 7.55 (d, J = 1.57 Hz, 1H), 7.48 (t, J = 7.83 Hz, 1H), 7.44 (dd, J = 1.96, 8.22 Hz, 1H), 7.23 (t, J = 7.63 Hz, 1H), 7.01 (d, J = 8.22 Hz, 1H), 6.88 (d, J = 8.61 Hz, 1H), 3.92 (s, 3H).

(B) 4-(2-Trifluoromethylphenoxy)-3-methoxybenzaldehyde was condensed with 2,4-thiazolidinedione according to general procedure D. The reaction mixture was concentrated under reduced pressure, and the solid orange residue was purified by flash chromatography (DCM) to afford the title compound as pale yellow needles (from MeOH). Yield: 76%. ^{1}H NMR (400 MHz, DMSO-d_6) δ 12.66 (br s, 1H), 7.84 (s, 1H), 7.77 (d, J = 6.65 Hz, 1H), 7.59 (t, J = 7.24 Hz, 1H), 7.47 (d, J = 1.96 Hz, 1H), 7.27 (t, J = 7.63 Hz, 1H), 7.23 (dd, J = 1.96, 8.61 Hz, 1H), 7.17 (d, J = 8.22 Hz, 1H), 6.85 (d, J = 8.22 Hz, 1H), 3.81 (s, 3H). MS (APCI+) m/z 394.9 [$(M)^{+\bullet}$]. t_R = 7.35 min (95.7%).

2-[4-(2,4-Dioxothiazolidin-5-ylidenemethyl)-2-methoxyphenoxy]-5-trifluoromethylbenzoic Acid Methyl Ester (31). (A) 2-Fluoro-5-trifluoromethylbenzoic acid methyl ester was reacted with vanillin according to general procedure A to afford 2-(4-formyl-2-methoxyphenoxy)-5-trifluoromethylbenzoic acid methyl ester as a pale yellow oil. Yield: 94%. ^{1}H NMR (400 MHz, $CDCl_3$) δ 9.93 (s, 1H), 8.24 (d, J = 1.96 Hz, 1H), 7.69 (dd, J = 2.35, 8.61 Hz, 1H), 7.55 (d, J = 1.56 Hz, 1H), 7.44 (dd, J = 1.76, 8.02 Hz, 1H), 7.00 (d, J = 8.22 Hz, 1H), 6.97 (d, J = 8.61 Hz, 1H), 3.89−3.94 (m, 3H), 3.83−3.88 (m, 3H).

(B) 2-(4-Formyl-2-methoxyphenoxy)-5-trifluoromethylbenzoic acid methyl ester was condensed with 2,4-thiazolidinedione according to general procedure B to afford the title compound as a canary yellow solid. Yield: 78%. ^{1}H NMR (400 MHz, $CDCl_3$) δ 8.24 (d, J = 2.31 Hz, 1 H), 7.82 (s, 1 H), 7.68 (dd, J = 8.57, 2.31 Hz, 1 H), 7.06−7.18 (m, 2 H), 6.97−7.06 (m, 1 H), 6.93

(d, J = 8.57 Hz, 1 H), 3.91 (s, 3 H), 3.89 (s, 3 H). MS (APCI+) m/z 453.0 [$(M)^{+\bullet}$]. t_R = 7.29 min (98.9%).

4-[4-(2,4-Dioxothiazolidin-5-ylidenemethyl)-2-methoxyphenoxy]-2-trifluoromethylbenzoic Acid Methyl Ester (32). (A) Methyl 4-fluoro-2-trifluoromethylbenzoate was reacted with vanillin according to general procedure A to afford 4-(4-formyl-2-methoxyphenoxy)-2-trifluoromethylbenzoic acid methyl ester as a white crystalline solid. Yield: 88%. ^{1}H NMR (400 MHz, $CDCl_3$) δ 9.98 (s, 1H), 7.84 (d, J = 8.61 Hz, 1H), 7.57 (d, J = 1.57 Hz, 1H), 7.52 (dd, J = 1.76, 8.02 Hz, 1H), 7.34 (d, J = 2.35 Hz, 1H), 7.19 (d, J = 8.22 Hz, 1H), 7.07 (dd, J = 2.54, 8.41 Hz, 1H), 3.93 (s, 3H), 3.89 (s, 3H).

(B) 4-(4-Formyl-2-methoxyphenoxy)-2-trifluoromethylbenzoic acid methyl ester was condensed with 2,4-thiazolidinedione according to general procedure D to afford the title compound as fine orange-yellow crystals (from MeOH). Yield: 31%. ^{1}H NMR (400 MHz, DMSO-d_6) δ 12.68 (br s, 1H), 7.84−7.89 (m, 2H), 7.50 (d, J = 1.96 Hz, 1H), 7.36−7.41 (m, 2H), 7.27 (dd, J = 1.96, 8.22 Hz, 1H), 7.16 (dd, J = 2.74, 8.61 Hz, 1H), 3.84 (s, 3H), 3.80 (s, 3H). MS (APCI+) m/z 452.9 [$(M)^{+\bullet}$]. t_R = 7.35 min (99.3%).

4-[4-(2,4-Dioxothiazolidin-5-ylidenemethyl)-2-methoxyphenoxy]-2-methylbenzonitrile (33). (A) 4-Fluoro-3-methylbenzonitrile was reacted with vanillin according to general procedure A to afford 4-(4-formyl-2-methoxyphenoxy)-2-methylbenzonitrile as a white crystalline solid. Yield: 28%. ^{1}H NMR (400 MHz, $CDCl_3$) δ 9.97 (s, 1H), 7.57 (s, 1H), 7.55 (d, J = 6.65 Hz, 1H), 7.50 (dd, J = 1.76, 8.02 Hz, 1H), 7.16 (d, J = 8.22 Hz, 1H), 6.87 (d, J = 2.35 Hz, 1H), 6.80 (dd, J = 2.54, 8.41 Hz, 1H), 3.90 (s, 3H), 2.51 (s, 3H).

(B) 4-(4-Formyl-2-methoxyphenoxy)-2-methylbenzonitrile was condensed with 2,4-thiazolidinedione according to general procedure C to afford the title compound as a light tan-colored solid. Yield: 33%. ^{1}H NMR (400 MHz, $CDCl_3$) δ 12.62 (br s, 1H), 7.82 (s, 1H), 7.70 (d, J = 8.61 Hz, 1H), 7.45 (d, J = 1.96 Hz, 1H), 7.28 (d, J = 8.22 Hz, 1H), 7.23 (dd, J = 1.96, 8.22 Hz, 1H), 6.95 (d, J = 2.35 Hz, 1H), 6.79 (dd, J = 2.74, 8.61 Hz, 1H), 3.78 (s, 3H), 2.41 (s, 3H). MS (APCI+) m/z 365.9 [$(M)^{+\bullet}$]. t_R = 6.87 min (100%).

4-[4-(2,4-Dioxothiazolidin-5-ylidenemethyl)-2-methoxyphenoxy]-3-methylbenzonitrile (34). (A) 4-Fluoro-3-methylbenzonitrile was reacted with vanillin according to general procedure A (only a partial reaction took place after several days at 110 °C) to afford 4-(4-formyl-2-methoxyphenoxy)-3-methylbenzonitrile as a white solid. Yield: 38%. ^{1}H NMR (400 MHz, $CDCl_3$) δ 9.95 (s, 1H), 7.54−7.58 (m, 2H), 7.47 (dd, J = 1.96, 8.22 Hz, 1H), 7.43 (dd, J = 2.15, 8.41 Hz, 1H), 7.01 (d, J = 7.83 Hz, 1H), 6.74 (d, J = 8.22 Hz, 1H), 3.90 (s, 3H), 2.36 (s, 3H).

(B) 4-(4-Formyl-2-methoxyphenoxy)-3-methylbenzonitrile was condensed with 2,4-thiazolidinedione according to general procedure D to afford the title compound as small bright yellow crystals. Yield: 78%. ^{1}H NMR (400 MHz, DMSO-d_6) δ 12.66 (br s, 1H), 7.84 (s, 1H), 7.80 (d, J = 1.17 Hz, 1H), 7.59 (dd, J = 2.15, 8.41 Hz, 1H), 7.47 (s, 1H), 7.23 (s, 2H), 6.67 (d, J = 8.22 Hz, 1H), 3.80 (s, 3H), 2.31 (s, 3H). MS (APCI+) m/z 366.1 [$(M)^{+\bullet}$]. t_R = 5.55 min (100%).

4-[4-(2,4-Dioxothiazolidin-5-ylidenemethyl)-2-methoxyphenoxy]-phthalonitrile (35). (A) 4-Fluorophthalonitrile was reacted with vanillin according to general procedure A to afford 4-(4-formyl-2-methoxyphenoxy)phthalonitrile as a white solid. Yield: 62%. ^{1}H NMR (400 MHz, $CDCl_3$) δ 10.01 (s, 1H), 7.73 (d, J = 8.61 Hz, 1H), 7.59−7.61 (m, 1H), 7.57 (dd, J = 1.57, 7.83 Hz, 1H), 7.29 (d, J = 7.83 Hz, 1H), 7.22 (d, J = 2.35 Hz, 1H), 7.19 (dd, J = 2.74, 8.61 Hz, 1H), 3.86 (s, 3H).

(B) 4-(4-Formyl-2-methoxyphenoxy)phthalonitrile was condensed with 2,4-thiazolidinedione according to general procedure C to afford the title compound as a light yellow solid. Yield: 63%. ^{1}H NMR (400 MHz, DMSO-d_6) δ 12.68 (br s, 1H), 8.05 (d, J = 9.00 Hz, 1H), 7.84 (s, 1H), 7.76 (d, J = 2.74 Hz, 1H), 7.49 (d, J = 1.57 Hz, 1H), 7.37 (d, J = 8.22 Hz, 1H), 7.30 (dd, J = 2.54, 8.80 Hz, 1H), 7.26 (dd, J = 1.76, 8.41 Hz, 1H), 3.77 (s, 3H). MS (APCI+) m/z 376.9 [$(M)^{+\bullet}$]. t_R = 6.60 min (99.3%).

2-Chloro-4-[4-(2,4-dioxothiazolidin-5-ylidenemethyl)-2-methoxyphenoxy]benzonitrile (36). (A) 2-Chloro-4-fluorobenzonitrile was reacted with vanillin according to general procedure A to afford 2-chloro-4-(4-formyl-2-methoxyphenoxy)benzonitrile as a cream-colored powder. Yield: 97%. ^{1}H NMR (400 MHz, $CDCl_3$) δ 9.99 (s, 1H), 7.61 (d, J = 9.00 Hz, 1H), 7.58 (d, J = 1.96 Hz, 1H), 7.54 (dd, J = 1.96, 7.83 Hz, 1H), 7.24 (d, J = 7.83 Hz, 1H), 7.01 (d, J = 2.35 Hz, 1H), 6.88 (dd, J = 2.35, 8.61 Hz, 1H), 3.88 (s, 3H).

(B) 2-Chloro-4-(4-formyl-2-methoxyphenoxy)benzonitrile was condensed with 2,4-thiazolidinedione according to general procedure C to afford the title compound as an off-white solid. Yield: 91%. ^{1}H NMR (400 MHz, DMSO-d_6) δ 12.64 (br s, 1H), 7.90 (d, J = 8.61 Hz, 1H), 7.83 (s, 1H), 7.47 (d, J = 1.96 Hz, 1H), 7.35 (d, J = 8.61 Hz, 1H), 7.22−7.29 (m, 2H), 6.95 (dd, J = 2.54, 8.80 Hz, 1H), 3.78 (s, 3H). MS (APCI+) m/z 385.9 [$(M)^{+\bullet}$]. t_R = 7.10 min (98.6%).

4-[4-(2,4-Dioxothiazolidin-5-ylidenemethyl)-2-methoxyphenoxy]-benzonitrile (37). (A) 4-Fluorobenzonitrile was reacted with vanillin according to general procedure A to afford 4-(4-formyl-2-methoxyphenoxy)benzonitrile as a sticky pink-tinted white solid. Yield: 82%. ^{1}H NMR (400 MHz, $CDCl_3$) δ 9.96 (s, 1H), 7.59−7.64 (m, 2H), 7.56 (d, J = 1.96 Hz, 1H), 7.50 (dd, J = 1.76, 8.02 Hz, 1H), 7.18 (d, J = 8.22 Hz, 1H), 6.96−7.02 (m, 2H), 3.87 (s, 3H).

(B) 4-(4-Formyl-2-methoxyphenoxy)benzonitrile was condensed with 2,4-thiazolidinedione according to general procedure C to afford the title compound as a cream-colored solid. Yield: 88%. ^{1}H NMR (300 MHz, DMSO-d_6) δ 12.67 (br s, 1H), 7.73−7.84 (m, 3H), 7.46 (d, J = 1.98 Hz, 1H), 7.28−7.35 (m, 1H), 7.21−7.28 (m, 1H), 6.97−7.06 (m, 2H), 3.78 (s, 3H). MS (APCI+) m/z 351.9 [$(M)^{+\bullet}$]. t_R = 6.60 min (100%).

4-[4-(2,4-Dioxothiazolidin-5-ylidenemethyl)-2-methoxyphenoxy]-naphthalene-1-carbonitrile (38). (A) 4-Fluoronaphthonitrile was reacted with vanillin according to general procedure A to afford 4-(4-formyl-2-methoxyphenoxy)naphthalene-1-carbonitrile as a cream-colored solid. Yield: 86%. ^{1}H NMR (400 MHz, $CDCl_3$) δ 9.99 (s, 1H), 8.43 (d, J = 8.22 Hz, 1H), 8.26 (d, J = 8.22 Hz, 1H), 7.74−7.82 (m, 2H), 7.65−7.71 (m, 1H), 7.61 (d, J = 1.96 Hz, 1H), 7.53 (dd, J = 1.96, 7.83 Hz, 1H), 7.22 (d, J = 8.22 Hz, 1H), 6.68 (d, J = 8.22 Hz, 1H), 3.88 (s, 3H).

(B) 4-(4-Formyl-2-methoxyphenoxy)naphthalene-1-carbonitrile was condensed with 2,4-thiazolidinedione according to general procedure C to afford the title compound as a yellow-tinted cream-colored solid. Mp: 255−258 °C (dec). Yield: 93%. ^{1}H NMR (400 MHz, acetone-d_6) δ 8.53 (d, J = 8.61 Hz, 1H), 8.20 (d, J = 8.22 Hz, 1H), 7.95 (d, J = 7.83 Hz, 1H), 7.89 (t, J = 7.63 Hz, 1H), 7.74−7.82 (m, 1H), 7.66 (s, 1H), 7.47 (d, J = 1.96 Hz, 1H), 7.38 (d, J = 8.22 Hz, 1H), 7.33 (dd, J = 1.96, 8.22 Hz, 1H), 6.74 (d, J = 8.22 Hz, 1H), 3.86 (s, 3H). MS (APCI+) m/z 402.0 [$(M)^{+\bullet}$]. t_R = 7.59 min (100%). Anal. Calcd for $C_{22}H_{14}N_2O_4S$: C, 65.66%; H, 3.51%; N, 6.96%. Found: C, 65.96%; H, 3.48%; N, 6.96%.

4-[4-(2,4-Dioxothiazolidin-5-ylidenemethyl)-2-methoxyphenoxy]-naphthalene-1-carboxylic Acid Methyl Ester (39). (A) Methyl 4-fluoronaphthoate was reacted with vanillin according to general procedure A to afford methyl 4-(4-formyl-2-methoxyphenoxy)naphthalene-1-carboxylate as a white solid. Yield: 10%. ^{1}H NMR (400 MHz, acetone- d_6) δ 10.04 (s, 1H), 9.08 (br d, J = 9.00 Hz, 1H), 8.42 (br d, J = 7.83 Hz, 1H), 8.17 (d, J = 8.22 Hz, 1H), 7.71−7.78 (m, 2H), 7.64−7.70 (m, 2H), 7.38 (d, J = 7.83 Hz, 1H), 6.77 (d, J = 8.22 Hz, 1H), 3.94 (s, 3H), 3.90 (s, 3H).

(B) Methyl 4-(4-formyl-2-methoxyphenoxy)naphthalene-1-carboxylate was condensed with 2,4-thiazolidinedione according to general procedure E to afford the title compound as an off-white solid. Yield: 30%. ^{1}H NMR (400 MHz, DMSO-d_6) δ 8.93 (d, J = 8.61 Hz, 1H), 8.40 (d, J = 8.22 Hz, 1H), 8.09 (d, J = 8.22 Hz, 1H), 7.70−7.77 (m, 1H), 7.61−7.69 (m, 1H), 7.41 (d, J = 1.96 Hz, 1H), 7.36 (s, 1H), 7.29 (d, J = 8.22 Hz, 1H), 7.23 (dd, J = 1.96, 8.22 Hz, 1H), 6.61 (d, J = 8.22 Hz, 1H), 3.88 (s, 3H), 3.74

(s, 3H). MS (APCI+) m/z 434.9 9 [$(M)^{+\bullet}$] (minor); 421.9 $(M - CH_3 + 2H)^+$. $t_R = 7.71$ min (100%).

4-[4-(2,4-Dioxothiazolidin-5-ylmethyl)-2-methoxyphenoxy]-2-trifluoromethylbenzoic Acid Methyl Ester (40). To an ice-cold solution of $CoCl_2 \cdot 6H_2O$ (2.5 mg, 0.01 mmol) and dimethylglyoxime (13 mg, 0.11 mmol) in water (6 mL) was added a drop of 1 N NaOH, followed by $NaBH_4$ (50 mg, 1.32 mmol). To the resulting dark olive-amber solution was added, over a 10 min period, a solution of 4-[4-(2,4-dioxothiazolidin-5-ylidenemethyl)-2-methoxyphenoxy]-2-trifluoromethylbenzoic acid methyl ester (**32**) (90 mg, 0.2 mmol) in a mixture of THF (3 mL) and DMF (0.25 mL). The solution was allowed to gradually warm to room temperature and stirred overnight. The mixture was then acidified to pH 5 with HOAc, diluted with water (6 mL), extracted with CH_2CH_2 (3 × 5 mL), dried (Na_2SO_4), and concentrated under reduced pressure. The residue was purified by silica gel chromatography, eluting with CH_2CH_2−MeOH (100:1) to afford a colorless film, which crystallized from ether/hexane to afford the title compound as white granules (75 mg, 83%). ^{1}H NMR (400 MHz, DMSO-d_6) δ 12.11 (s, 1H), 7.86 (d, J = 8.61 Hz, 1H), 7.26 (d, J = 2.35 Hz, 1H), 7.14−7.22 (m, 2H), 7.06 (dd, J = 8.61, 2.74 Hz, 1H), 6.93 (dd, J = 8.02, 1.76 Hz, 1H), 5.00 (dd, J = 9.59, 4.50 Hz, 1H), 3.83 (s, 3H), 3.72 (s, 3H), 3.46 (dd, J = 14.09, 4.30 Hz, 1H), 3.15 (dd, J = 14.09, 9.78 Hz, 1H). MS (APCI+) m/z 454.8 [$(M)^{+\bullet}$]. $t_R = 6.99$ min (100%).

Biological Procedures. (1) FRET Assays. Time-resolved fluorescence resonance energy transfer (TR-FRET) experiments were performed to examine the functional response of ERRα ligands. The components of this homogeneous secondary assay included the ^{6}His-tagged- ERRα LBD, a GST-labeled-hSRC2 coactivator polypeptide, and a fluorescent donor/acceptor pair from Cisbio Bioassays (Bedford, MA) using both an α-GST europium cryptate (Eu) label and an α^{6}His-XL665 (allophycocyanin) fluorophore.

For TR-FRET measurements, the mixture was buffered in 25 mM Tris, pH 8, 2.5 mM Hepes, 20 mM KCl, 1 mM DTT, and 0.05 mg/mL BSA (−lipids). The final concentrations of reagents were 6 nM ERRα LBD, 6 nM GST-SRC-2 peptide, 30 nM Eu cryptate, and 7.5 nM XL665. Reactions were allowed to reach equilibrium at 25 °C for 4−18 h before collecting data on the Analyst from LJL Biosystems (Molecular Devices, Sunnyvale, CA). As a time-resolved method, the samples were excited at 340 nM and emission was collected for 1 ms at both 615 and 665 nm with delays of 400 and 75 μs, respectively. Dose response curves were fitted using a hyperbolic equation, and the data reported are the average of three independent experiments.

A similar assay was used to evaluate the functional response of **29** against the ERRγ receptor, as previously described.[47]

(2) Two-Hybrid Reporter Assay (ERRα). Cell based reporter assays were used to determine the functional response of the ERRα ligands. Transfections were performed in HEK293E cells that were maintained in DMEM supplemented in glutamine and 10% FBS. Co-transfection of 4 μg of a luciferase reporter plasmid and 4 μg each of pACT-ERRα and pBIND-Gal4-SRC2 plasmids per T-75 flask was done using Lipofectamine 2000 per the manufacturer's instructions. Twenty-four hours post-transfection, the cells were seeded in 96-well plates at a density of 50 000 cells per well in assay media (DMEM phenol free, 5% charcoal stripped FBS). The cells were allowed to adhere to the bottom of the wells approximately 5 h after seeding, and the compounds were dosed such that the final concentration of DMSO was kept below 0.3%. After 24 h of compound treatment, cells were lysed and treated with the Promega Dual-Glo system. Firefly luciferase activity was read using a luminescence plate reader, and data were normalized against Renilla luciferase activity. Data were fitted using subroutines available from GraphPad.

(3) Two-Hybrid Reporter Assay (ERRγ). Transfections were performed in HEK293E cells that were maintained in DMEM supplemented in glutamine and 10% FBS. Co-transfection of 4 μg of a luciferase reporter plasmid and 4 μg each of pBIND-Gal4-ERRγ and pACT-SRC2 plasmids per T-75 flask was done using Lipofectamine 2000 per manufacturer's instructions. Twenty-four hours post-transfection, the cells were seeded in 96-well plates at a density of 50 000 cells per well in assay media (DMEM phenol free, 5% charcoal stripped FBS). The cells were allowed to adhere to the bottom of the wells approximately 5 h after seeding, and the compounds were dosed such that the final concentration of DMSO was kept below 0.3%. After 24 h of compound treatment, cells were lysed and treated with the Promega Dual-Glo system. Firefly luciferase activity was read using a luminescence plate reader, and data were normalized against Renilla luciferase activity. Data were fitted using subroutines available from GraphPad.

(4) Monohybrid Reporter Assays (PPARα, PPARγ, PPARδ, RXRα). Transfections were performed in HEK293E cells that were maintained in DMEM supplemented in glutamine and 10% FBS. Co-transfection of 4 μg of a luciferase reporter plasmid and 4 μg of each pM-Gal4-LBD (corresponding to the respective receptor) per T-75 flask was carried out using Lipofectamine 2000 as per manufacturer's instructions. Twenty-four hours post-transfection, the cells were seeded in 96-well plates at a density of 50 000 cells per well in assay media (DMEM phenol free, 5% charcoal stripped FBS). The cells were allowed to adhere to the bottom of the wells approximately 5 h after seeding, and the compounds were dosed such that the final concentration of DMSO was kept below 0.3%. After 24 h of compound treatment, cells were lysed and treated with the Promega luciferase system. Data were fitted using subroutines available from GraphPad. To test the ERRα ligands in the antagonist format, the receptors were assayed in the presence of the appropriate agonist compounds (GAL-PPARα with GW7647, GAL-PPARγ with rosiglitazone, GAL-PPARδ with GW0742, GAL-RXRα with bexarotene).

(5) ERβ Reporter Assay. The ligand binding domain of ERβ fused to a ZFP (zinc finger protein) was employed to characterize the functional activity of the compound in a cellular reporter assay. The ZFP was engineered to bind to the promoter of the alkaline phosphatase (ALPL) gene. Stable cell lines were generated in HEK293 cells under the selection of G418. The cells were seeded in 96-well plates at density of 10 000 cells per well in assay media (DMEM phenol free, 5% charcoal stripped FBS). The cells were allowed to adhere to the bottom of the wells approximately 5 h after seeding, and the compounds were dosed such that the final concentration of DMSO was kept below 0.3%. When compounds were tested in the antagonist mode, 10 nM E2 was added to the media. After 24 h of compound treatment, cells were lysed with reporter lysis buffer and alkaline phosphatase activity was measured with secreted embryonic alkaline phosphatase assay as per manufacturer's instructions (SEAP reagent, Promega). Data were fitted using subroutines available from GraphPad.

(6) MCF7 Proliferation Assay (ERα). Briefly, MCF-7 cells were allowed to adapt in dextran-treated charcoal-stripped serum and phenol free DMEM for 5 days. Then 1K cells per well were plated in a 96-well dish in a final volume of 50 μL. Compounds to be tested in the agonist mode were added at 2 times their final concentration (50 μL) after 5 h. Compounds to be treated in the antagonist mode were prepared similarly, and 10 nM 3,17β-estradiol was also added to the culture media. The final concentration of DMSO was maintained at 0.5%. Cell density/viability was measured at days 0, 3, and 6 using a commercial CellTiter-Glo reagent per manufacturer's instructions (Promega).

(7) Structural Determination of ERRα-29 Complex. The LBD of ERRα (amino acids 289−519, Swiss-Prot P11474)[52] was subcloned into pDEST with an N-terminal His tag and the cleavable PreSission site. The plasmid was co-transfected with linearized baculovirus DNA into insect cells, and the baculovirus was amplified and purified from plaques from a titer (1−2) × 10^8 PFU/mL. Sf9 cells were maintained in ESF921 media and grown in 2 L Erlenmeyer flasks at 27 °C. The insect

cells at a cell density of 1.5×10^6 cells/mL were infected with the baculovirus at a multiplicity of infection of 1, and cells were harvested, 3 days after infection, by centrifugation at 1200*g*, rinsed with PBS supplemented with protease inhibitors, and stored at −80 °C until further use. Expression level of the protein was confirmed by Western blots using an α-His antibody. For purification the cells were lysed into 25 mM Tris-HCl, pH 8.0, 0.5 M NaCl, and 10 mM β-mercaptoethanol, using an Emulsiflex-C5 French press (Avestin). Insoluble material was removed by centrifugation at 40000*g* for 1 h. Clarified homogenate was applied on a Ni-NTA column, and after application of an imidazole gradient, the protein was eluted. The protein was dialyzed against 25 mM Tris-HCl, pH 8.0, 50 mM NaCl, and 5 mM dithiothreitol (DTT) and further purified on an anion exchange column by applying a linear gradient of NaCl from 50 to 1000 mM. Protein purity was greater than 95% as judged by SDS−PAGE chromatography. The aggregation state of the protein was confirmed by dynamic light scattering. Protein was dialyzed in 25 mM Tris-HCl, pH 7.5, 0.2 M NaCl, 1 mM EDTA, and 1 mM DTT, aliquoted, and stored at −80 °C until further use. Purified human ERRα-LBD was buffer exchanged in 25 mM Tris, pH 8, 0.3 M NaCl, 5 mM DTT, and 5% glycerol, complexed with the **29** in a 1:2 molar ratio, and concentrated to ∼17 mg/mL. The protein was screened for crystallization using the hanging-drop vapor diffusion method. The reservoir contained 650 μL of the precipitant solution, and the 2 mL hanging drop consisted of a 1:1 protein-to-precipitant solution ratio. Crystals formed at 4 °C from a solution containing 1.4 M ammonium sulfate, 100 mM PIPES, pH 6.5, and 200 mM sodium thiocyanate. The crystals were transferred to a cryoprotectant solution containing 1.4 M ammonium sulfate, 100 mM PIPES, pH 6.5, 200 mM sodium thiocyanate, and 25% glycerol. The crystals were then mounted and quickly frozen by immersion in liquid nitrogen. X-ray diffraction data to a resolution to 2.0 Å were collected on a Bruker AXS Proteum 6000 detector. Diffraction data were indexed, integrated, and scaled using the Proteum Processing Program suite from Bruker AXS. Under these conditions, the crystals belong to the $P6_522$ space group, with unit cell parameters $a=b=103$ Å, $c=110$ Å, $\alpha=\beta=90°$, and $\gamma=120°$. The structure was determined by molecular replacement with CNX[62] using one molecule from the homodimer structure of ERRα with the PGC-1α peptide (PDB code 1XB7) as the search model.[32] Model building was performed using O[63] and Coot.[64] Refinement and map calculations were carried out using PHENIX.[65] The final structure was refined to an R_{factor} of 22.7 and R_{free} of 26.7. The atomic coordinates and structure factors (PDB code 3K6P) have been deposited in the Protein Data Bank Research Collaboratory for Structural Bioinformatics, Rutgers University, New Brunswick, NJ (http://www.rcsb.org/).

(8) Characterization of the ERRα-Ligand Complexes. Formation of the ERRα-**29** complex was carried out by mixing equal volumes of the ERRα LBD (1 μM) and **29** (2 μM) in HEPES buffer. Aliquots (20 μL) of the complex solution were transferred at defined time intervals (0, 1, 2, 5, 10, 30, 55, and 120 min) into a solution of 10% CH_3CN containing 0.1% TFA (100 μL) to quench the reaction. LCMS analysis (50 μL aliquot) was performed on an Agilent 1100 LC system that was coupled with an Agilent MSD time-of flight (TOF) mass spectrometer. Software provided by the vendor (Agilent BioConfirm software, version A02.00) was used to deconvolute the ESI positive ion quadrupole TOF spectra. For competition experiments, the above ERRα-**29** mixture (100 μL) was equilibrated for 1 h to allow for complete complex formation. An equal volume of competing ligand **27** (40 μM in HEPES buffer) was then added, and aliquots were removed and processed as described above. Final concentrations of ligand, protein, and competing ligand were 1, 0.5, and 20 μM, respectively. All experiments were carried out in buffer containing 25 mM HEPES, pH 7.9, 200 mM KCl, and 3% DMSO at 37 °C.

Pharmacokinetic Studies. (1) Male Sprague−Dawley rats (250−300 g) were dosed with test compound intravenously at 2 mg/kg and by oral gavage at 10 mg/kg. Blood samples (300−400 μL) were then obtained via orbital sinus puncture at 0.08 (iv only), 0.25, 0.5, 1, 2, 4, 6, 8, and 24 h time points and collected into heparinized tubes. Blood samples were centrifuged for cell removal, and the plasma supernatant was then transferred to a clean vial, placed on dry ice, and subsequently stored in a −70 °C freezer prior to analysis. Test sample concentrations were determined by LCMS. Pharmacokinetic parameters were calculated using noncompartmental models by the WinNonLin software package (Pharsight). Test compounds were formulated as follows. **5** and **38** (iv and po): 2% NMP and 20% HPβCD (pH adjusted to 7.9 with 1 N NaOH). **29** (iv): 2% NMP and 10% Solutol (pH 5.5). **29** (po): 15% vitamin E-TPGS/30% PEG400 (1:2, w/w) (pH 7.6).

(2) Male CD1 mice (30 to 45 g) were dosed intravenously at 2 mg/kg and orally at 10 mg/kg with **29** formulated in a solution of 2% NMP and 10% Solutol in water. Blood samples were obtained at 0.083 (iv only), 0.25, 0.5, 1, 2, 4, 6, and 7 h time points by terminal bleeds (three and four animals per time point, iv and po, respectively) and were processed and subjected to LC/MS analysis (vide supra).

(3) Female Beagle dogs (8.1−11.8 kg) were dosed intravenously at 2 mg/kg and orally at 10 mg/kg with **29** in a solution of 5% NMP and 20% HPβCD. Blood samples (1−3 mL) were obtained via jugular or saphenous venipuncture at 0.083 (iv only), 0.25, 0.5, 1, 2, 4, 7, 24, 28, 31, and 48 h time points and collected, processed, and subjected to LC/MS analysis (vide supra).

(4) Female cynomolgus monkeys (3.0−4.0 kg) were dosed intravenously via the saphenous or cephalic vein at 2 mg/kg and orally via stomach intubation at 10 mg/kg with **29** in 20% HPβCD. The iv formulation was an opaque yellow homogeneous solution. The oral formulation was a yellow uniform suspension. Blood samples (1−3 mL) were obtained via femoral or saphenous venipuncture at 0.083, 0.25, 0.5, 1, 2.5, 4, 7, and 24 h time points (iv dosing) and at 0.25, 0.5, 1, 2.5, 4, 7, 24, 28, 31, 48, 52, 55, and 72 h time points (po dosing). Collection, processing, and LCMS analyses were carried out as described above.

Pharmacological Studies. (1) Thirty AKR/J male mice (21 g) were received at 7 weeks of age and allowed to acclimate for 1 week and then placed on high fat diet (45% of the calories from fat) for 5 weeks. Animals were treated for 5 days with **29** (3 and 30 mg/kg, formulated in 15% vitamin E-TPGS, 30% PEG-400, and 55% water) given orally, twice a day. Food intake was measured on day 4. On day 5, prior to necropsies, body weight was recorded and body composition was measured by Q-NMR. Animals were anesthetized with carbon dioxide and blood was collected by cardiac puncture. Plasma was obtained by centrifugation and used to determine circulating insulin levels and clinical chemistries, including liver function tests, using commercially available kits as per manufacturers' instructions. Several tissues were harvested, frozen in liquid nitrogen, and stored at −80 °C for further use.

(2) Forty C57BL/6 male mice were received at 7 weeks of age, allowed to acclimate for 1 week, placed on high fat diet (test diet 58Y1, 60% of the calories from fat) for 6 weeks, and then single housed on the same diet for an additional 5 weeks. Body mass composition and insulin were used to randomize the animals into three groups. Mice were dosed once a day with vehicle or **29** (10 and 30 mg/kg) for 18 days. The vehicle used in this study consisted of 15% vitamin E-TPGS, 30% PEG400, and 55% water. Ten additional animals were maintained on a low fat diet (4% calories from fat) and during the course of the study were given vehicle orally once a day. Blood was collected from the tail to evaluate glucose, triglyceride, FFA, and insulin levels. Body weight and body composition were also recorded. On day 14, an OGTT was performed to determine glucose disposal rates. The mice were fasted overnight and received a 2 g/kg oral gavage of

glucose. Tail vein blood was collected, and glucose levels were measured at the 0, 15, 30, 60, and 120 min time points. Upon necropsy animals were bled through the orbital sinus under CO_2/O_2 anesthesia and sacrificed, and several tissues were collected and frozen in liquid nitrogen for storage at −80 °C for further use. Serum plasma samples were prepared by centrifugation in EDTA-containing tubes, and the supernatants were transferred to 96-well plates and stored at −80 °C.

(3) Fifty ZDF *fa*/*fa* male rats were received at 4 weeks of age and allowed to acclimate for 1 week. At 5 weeks of age, the animals were single-housed in cages in a temperature-controlled room with 12 h light/dark cycle. They were allowed ad libitum access to water and food, and throughout the study they were maintained on a Purina 5008 diet. Animals were sorted into five groups based primarily on glucose levels and secondarily on body weight (average fed glucose levels and body weight at 7 weeks of age were 488 mg/dL and 282 g, respectively). Animals in three groups were given **29** orally once a day for 12 days in the morning at 10 mg/kg. Two other groups were dosed daily with vehicle and rosiglitazone (10 mg/kg). The vehicle used for **29** in this study consisted of 15% vitamin E-TPGS, 30% PEG400, and 55% water (rosiglitazone vehicle: 0.5% methylcellulose). Body weight and total food intake were recorded at day 11. On day 12, an insulin tolerance test (ITT) was performed to evaluate peripheral insulin sensitivity. Briefly, animals were fasted for 4 h and then given an intraperitoneal injection of insulin (3 U/kg). Tail vein blood was collected, and blood glucose levels were measured at the 0, 15, 30, 60, and 120 min time points.

(4) Sixty-five ZDF *fa*/fa male rats were received, housed, and randomized into five groups, based on fed glucose levels and body weight vide supra. Average fed glucose levels and body weight at 7 weeks of age were 517 mg/dL and 293 g, respectively. The rats were dosed once a day with vehicle or **29** (0.08, 0.4, 2, and 10 mg/kg) for 25 days. The vehicle used in this study consisted of 15% vitamin E-TPGS, 30% PEG400, and 55% water. Food intake, body weight, glucose, insulin, triglyceride, and free fatty acid levels were monitored throughout the study using blood collected from tail vein bleeds. At day 22 of the study, an OGTT was performed to assess glucose disposal rates. On the day of necropsy, the rats were bled through the orbital sinus under CO_2/O_2 anesthesia. Animals were sacrificed, and several tissues were collected, frozen in liquid nitrogen, and stored at −80 °C. Serum plasma samples were prepared by centrifugation in EDTA-containing tubes, and the supernatants were transferred into 96-well plates and stored at −80 °C.

Acknowledgment. We thank Eric Asel for assistance in compound handling, Michael Kolpak for quantitative analyses of test sample solutions by ^{1}H NMR, and Karen Diloreto and Li Pan for assistance in the pharmacokinetic studies.

Supporting Information Available: A table of microarray gene ontology cluster analysis results from C57Bl/6 mouse liver; a table of gene expression analysis results of WT and ERRα −/− mice upon treatment with **29**. This material is available free of charge via the Internet at http://pubs.acs.org.

References

(1) Mangelsdorf, D. J.; Thummel, C.; Beato, M.; Herrlich, P.; Schutz, G.; Umesono, K.; Blumberg, B.; Kastner, P.; Mark, M.; Chambon, P.; Evans, R. M. The nuclear receptor superfamily: the second decade. *Cell* **1995**, *83*, 835–839.
(2) Rosenfeld, M. G.; Glass, C. K. Coregulator codes of transcriptional regulation by nuclear receptors. *J. Biol. Chem.* **2001**, *276*, 36865–36868.
(3) Giguere, V.; Yang, N.; Segui, P.; Evans, R. M. Identification of a new class of steroid hormone receptors. *Nature* **1988**, *331*, 91–94.
(4) Heard, D. J.; Norby, P. L.; Holloway, J.; Vissing, H. Human ERRγ, a third member of the estrogen receptor-related receptor (ERR) subfamily of orphan nuclear receptors: tissue-specific isoforms are expressed during development and in the adult. *Mol. Endocrinol.* **2000**, *14*, 382–392.
(5) Horard, B.; Vanacker, J. M. Estrogen receptor-related receptors: orphan receptors desperately seeking a ligand. *J. Mol. Endocrinol.* **2003**, *31*, 349–357.
(6) Lu, D.; Kiriyama, Y.; Lee, K. Y.; Giguere, V. Transcriptional regulation of the estrogen-inducible PS2 breast cancer marker gene by the ERR family of orphan nuclear receptors. *Cancer Res.* **2001**, *61*, 6755–6761.
(7) Shigeta, H.; Zuo, W.; Yang, N.; DiAugustine, R.; Teng, C. T. The mouse estrogen receptor-related orphan receptor alpha 1: molecular cloning and estrogen responsiveness. *J. Mol. Endocrinol.* **1997**, *19*, 299–309.
(8) Bonnelye, E.; Aubin, J. E. Differential expression of estrogen receptor-related receptor alpha and estrogen receptors alpha and beta in osteoblasts in vivo and in vitro. *J. Bone Miner. Res.* **2002**, *17*, 1392–1400.
(9) Bonnelye, E.; Vannacker, J. M.; Dittmar, T.; Begue, A.; Desbiens, X.; Denhardt, D. T.; Aubin, J. E.; Laudet, V.; Fournier, B. The ERR-1 orphan receptor is a transcriptional activator expressed during bone development. *Mol. Endocrinol.* **1997**, *11*, 905–916.
(10) Gaillard, S.; Dwyer, M. A.; McDonnell, D. P. Definition of the molecular basis for estrogen receptor-related receptor-alpha-cofactor interactions. *Mol. Endocrinol.* **2007**, *21*, 62–76.
(11) Kraus, R. J.; Ariazi, E. A.; Farrell, M. L.; Mertz, J. E. Estrogen-related receptor alpha 1 actively antagonizes estrogen receptor-regulated transcription in MCF-7 mammary cells. *J. Biol. Chem.* **2002**, *277*, 24826–24834.
(12) Ariazi, E. A.; Jordan, V. C. Estrogen-related receptors as emerging targets in cancer and metabolic disorders. *Curr. Top. Med. Chem.* **2006**, *6*, 203–215.
(13) Puigserver, P.; Spiegelman, B. M. Peroxisome proliferator-activated receptor-γ coactivator 1 α (PGC-1 α): transcriptional coactivator and metabolic regulator. *Endocr. Rev.* **2003**, *24*, 78–90.
(14) Schreiber, S. N.; Knutti, D.; Brogli, K.; Uhlmann, T.; Kralli, A. The transcriptional coactivator PGC-1 regulates the expression and activity of the orphan nuclear receptor estrogen-related receptor alpha (ERRalpha). *J. Biol. Chem.* **2003**, *278*, 9013–9018.
(15) Huss, J. M.; Kopp, R. P.; Kelly, D. P. Peroxisome proliferator-activated receptor coactivator-1α (PGC-1α) coactivates the cardiac-enriched nuclear receptors estrogen-related receptor-α and γ. *J. Biol. Chem.* **2002**, *277*, 40265–40274.
(16) Kamei, Y.; Ohizumi, H.; Fujitani, Y.; Nemoto, T.; Tanaka, T.; Takahashi, N.; Kawada, T.; Miyoshi, M; Ezaki, O.; Kakizuka, A. PPARgamma coactivator 1beta/ERR ligand 1 is an ERR protein ligand, whose expression induces a high-energy expenditure and antagonizes obesity. *Proc. Natl. Acad. Sci. U.S.A.* **2003**, *100*, 12378–12383.
(17) Laganiere, J.; Tremblay, G. B.; Dufour, C. R.; Giroux, S.; Rousseau, F.; Giguere, V. A polymorphic autoregulatory hormone response element in the human estrogen-related receptor α (ERRα) promoter dictates peroxisome proliferator-activated receptor γ coactivator-1α control of ERRα expression. *J. Biol. Chem.* **2004**, *279*, 18504–18510.
(18) Mootha, V. K.; Handschin, C.; Arlow, D.; Xie, X., St.; Pierre, J.; Sihag, S.; Yang, W.; Altshuler, D.; Puigserver, P.; Patterson, N.; Willy, P. J.; Schulman, I. G.; Heyman, R. A.; Lander, E. S.; Spiegelman, B. M. Errα and Gabpa/b specify PGC-1α-dependent oxidative phosphorylation gene expression that is altered in diabetic muscle. *Proc. Natl. Acad. Sci. U.S.A.* **2004**, *101*, 6570–6575.
(19) Christian, M.; White, R.; Parker, M. G. Metabolic regulation by the nuclear receptor corepressor RIP140. *Trends Endocrinol. Metab.* **2006**, *17*, 243–250.
(20) Christian, M.; Kiskinis, E.; Debevec, D.; Leonardsson, G.; White, R.; Parker, M. G. RIP 140-targeted repression of gene expression in adipocytes. *Mol. Cell. Biol.* **2005**, *25*, 9383–9391.
(21) Castet, A.; Herledan, A.; Bonnet, S.; Jalaguier, S.; Vanacker, J. M.; Cavailles, V. Receptor-interacting protein 140 differentially regulates estrogen receptor-related receptor transactivation depending on target genes. *Mol. Endocrinol.* **2006**, *20*, 1035–1047.
(22) Nichol, D.; Christian, M.; Steel, J. H.; White, R.; Parker, M. G. RIP140 expression is stimulated by estrogen-related receptor alpha during adipogenesis. *J. Biol. Chem.* **2006**, *281*, 32140–32147.
(23) Herzog, B.; Cardenas, J.; Hall, R. K.; Villena, J. A.; Budge, P. J.; Giguere, V.; Granner, D. K.; Kralli, A. Estrogen-related receptor α is a repressor of phosphoenolpyruvate carboxykinase gene transcription. *J. Biol. Chem.* **2006**, *281*, 99–106.
(24) Sladek, R.; Bader, J. A.; Giguere, V. The orphan nuclear receptor estrogen-related receptor α is a transcriptional regulator of the human medium-chain acyl coenzyme A dehydrogenase gene. *Mol. Cell. Biol.* **1997**, *17*, 5400–5409.

(25) Wende, A. R.; Huss, J. M.; Schaeffer, P. J.; Giguere, V.; Kelly, D. P. PGC-1alpha coactivates PDK4 gene expression via the orphan nuclear receptor ERRalpha: a mechanism for transcriptional control of muscle glucose metabolism. *Mol. Cell. Biol.* **2005**, *25*, 10684–10694.
(26) Araki, M.; Motojima, K. Identification of ERRalpha as a specific partner of PGC-1alpha for the activation of PDK4 gene expression in muscle. *FEBS J.* **2006**, *273*, 1669–1680.
(27) Zhang, Y.; Ma, K.; Sadana, P.; Chowdhury, F.; Gaillard, S.; Wang, F.; McDonnell, D. P.; Unterman, T. G.; Elam, M. B.; Park, E. A. Estrogen-related receptors stimulate pyruvate dehydrogenase kinase isoform 4 gene expression. *J. Biol. Chem.* **2006**, *281*, 39897–39906.
(28) Huang, B.; Wu, P.; Bowker-Kinley, M. M.; Harris, R. A. Regulation of pyruvate dehydrogenase kinase expression by peroxisome proliferator-activated receptor-α ligands, glucocorticoids and insulin. *Diabetes* **2002**, *51*, 276–283.
(29) Carrier, J. C.; Deblois, G.; Champigny, C.; Levy, E.; Giguere, V. Estrogen-related receptor alpha (ERRalpha) is a transcriptional regulator of apolipoprotein A-IV and controls lipid handling in the intestine. *J. Biol. Chem.* **2004**, *279*, 52052–52058.
(30) Luo, J.; Sladek, R.; Carrier, J.; Bader, J.; Richard, D.; Giguere, V. Reduced fat mass in mice lacking orphan nuclear receptor estrogen-related receptor α. *Mol. Cell. Biol.* **2003**, *23*, 7947–7956.
(31) Stein, R.; Way, J. M.; McDonnell, D. P.; Zuercher, W. J. Estrogen-related receptor α as a therapeutic target. *Drugs Future* **2006**, *31*, 427–436.
(32) Kallen, J.; Schlaeppi, J.-M.; Bitsch, F.; Filipuzzi, I.; Schilb, A.; Riou, V.; Graham, A.; Strauss, A.; Geiser, M.; Fournier, B. Evidence for ligand-independent transcriptional activation of the human estrogen-related receptor α (ERRα). *J. Biol. Chem.* **2004**, *279*, 49330–49337.
(33) Kallen, J.; Lattmann, R.; Beerli, R.; Blechschmidt, A.; Blommers, M. J. J.; Geiser, M.; Ottl, J.; Schlaeppi, J.-M.; Strauss, A.; Fournier, B. Crystal structure of human estrogen-related receptor α in complex with a synthetic inverse agonist reveals its novel molecular mechanism. *J. Biol. Chem.* **2007**, *282*, 23231–23239.
(34) Hyatt, S. M.; Lockamy, E. L.; Stein, R. A.; McDonnell, D. P.; Miller, A. B.; Orband-Miller, L. A.; Willson, T. M.; Zuercher, W. J. On the intractability of estrogen-related receptor α as a target for activation by small molecules. *J. Med. Chem.* **2007**, *50*, 6722–6724.
(35) Deuschle, U.; Heck, S.; Kober, I.; Bauer, U.; Balogh, I. NR3B1 Nuclear Receptor-Binding 3-Substituted Pyrazole Derivatives, and Therapeutic Uses. EP 1398029, 2004.
(36) Nolte, R. T.; Wang, L.; Orband-Miller, L. A.; Way, J. M.; Martin, J. J.; Roa, A. M.; Vela, L.; Miller, A. B.; Willson, T. M.; Zuercher, W. J. Identification and X-ray Crystal Structure of an ERR-alpha Inverse Agonist Reveals a New Mechanism of Nuclear Receptor Antagonism. *Abstracts of Papers*, 230th National Meeting of the American Chemical Society, Washington, DC, Aug 28 through Sep 1, 2005; American Chemical Society: Washington, DC, 2005; MEDI-474.
(37) Busch, B. B.; Stevens, W. C., Jr.; Martin, R.; Ordentlich, P.; Zhou, S.; Sapp, D. W.; Horlick, R. A.; Mohan, R. Identification of a selective inverse agonist for the orphan nuclear receptor estrogen-related receptor α. *J. Med. Chem.* **2004**, *47*, 5593–5596. Though selective among nuclear receptors for ERRα, weak agonist activity against PPARγ (EC_{50} = 1.3 μM; 15% efficacy vs agonist control) was also reported in this disclosure .
(38) Willy, P. J.; Murray, I. R.; Qian, J.; Busch, B. B.; Stevens, W. C., Jr.; Martin, R.; Mohan, R.; Zhou, S.; Ordentlich, P.; Wei, P.; Sapp, D. W.; Horlick, R. A.; Heyman, R. A. Regulation of PPARγ coactivator 1 α (PGC-1 α) signaling by an estrogen-related receptor α (ERR α) ligand. *Proc. Natl. Acad. Sci. U.S.A.* **2004**, *101*, 8912–8917.
(39) Pantoliano, M. W.; Petrella, E. C.; Kwasnoski, J. D.; Lobanov, V. S.; Myslik, J.; Graf, E.; Carver, T.; Asel, E.; Springer, B. A.; Lane, P.; Salemme, F. R. High-density miniaturized thermal shift assays as a general strategy for drug discovery. *J. Biomol. Screening* **2001**, *6*, 429–440.
(40) Tanis, S. P.; Parker, T. T.; Colca, J. R.; Fisher, R. M.; Kletzein, R. F. Synthesis and biological activity of metabolites of the antidiabetic antihyperglycemic agant pioglitazone. *J. Med. Chem.* **1996**, *39*, 5053–5063.
(41) Schultz, J. R.; Tu, H.; Lik, A.; Repa, J. J.; Medina, J. C.; Li, L.; Schwendner, S.; Wang, S.; Thoolen, M.; Mangelsdorf, D. J.; Lustig, K. D.; Shan, B. Role of LXRs in control of lipogenesis. *Genes Dev.* **2000**, *14*, 2831–2838.
(42) Kagechika, H.; Kawachi, E.; Hashimoto, Y.; Himi, T.; Shudo, K. Retinobenzoic acids. 1. Structure−activity relationships of aromatic amides with retinoidal activity. *J. Med. Chem.* **1988**, *31*, 2182–2192.
(43) Brown, P. J.; Stuart, L. W.; Hurley, K. P.; Lewis, M. C.; Winegar, D. A.; Wilson, J. G.; Wilkinson, W. O.; Ittoop, O. R.; Willson, T. M. Identification of a subtype selective human PPARalpha agonist through parallel-array synthesis. *Bioorg. Med. Chem. Lett.* **2001**, *11*, 1225–1227.
(44) Lehmann, J. M.; Moore, L. B.; Smith-Oliver, T. A.; Wilkison, W. O.; Willson, T. M.; Kliewer, S. A. An antidiabetic thiazolidinedione is a high affinity ligand for peroxisome proliferator-activated receptor gamma (PPAR gamma). *J. Biol. Chem.* **1995**, *270*, 12953–12956.
(45) Sznaidman, M. L.; Haffner, C. D.; Maloney, P. R.; Fivush, A.; Chao, E.; Goreham, D.; Sierra, M. L.; LeGrumelec, C.; Xu, H. E.; Montana, V. G.; Lambert, M. H.; Willson, T. M.; Oliver, W. R., Jr.; Sternbach, D. D. Novel selective small molecule agonists for peroxisome proliferator-activated receptor delta (PPARdelta)—synthesis and biological activity. *Bioorg. Med. Chem. Lett.* **2003**, *13*, 1517–1521.
(46) Boehm, M. F.; Zhang, L.; Badea, B. A.; White, S. K.; Mais, D. E.; Berger, E.; Suto, C. M.; Goldman, M. E.; Heyman, R. A. Synthesis and structure−activity relationships of novel retinoid X receptor-selective retinoids. *J. Med. Chem.* **1994**, *37*, 2930–2941.
(47) Abad, M. C.; Askari, H.; O'Neill, J.; Klinger, A. L.; Milligan, C.; Lewandowski, F.; Springer, B.; Spurlino, J.; Rentzeperis, D. Structural determination of estrogen-related receptor γ in the presence of phenol derivative compounds. *J. Steroid Biochem. Mol. Biol.* **2008**, *108*, 44–54 [Positive control: 4-hydroxytamoxifen (IC_{50} = 11 nM)] .
(48) PPARγ: Invitrogen PolarScreen PPAR Competitor Assay, Green (catalog no. PV3355), rosiglitazone (control), IC_{50} = 0.17 μM. ERα: Invitrogen PolarScreen ERalpha Competitor Assay, Green (catalog no. P2614); E2 (control), IC_{50} = 6.7 nM. ERβ: Invitrogen PolarScreen ERbeta Competitor Assay, Green (catalog no. P2615); E2 (control), IC_{50} = 7.8 nM.
(49) ERα: Invitrogen LanthaScreen TR-FRET ER alpha Coactivator Assay Kit (catalog no. PV4544); ERβ: Invitrogen LanthaScreen TR-FRET ER beta Coactivator Assay Kit (catalog no. PV4541); LXRα: Invitrogen LanthaScreen TR-FRET LXR alpha Coactivator Assay Kit (catalog no. PV4655); LXRβ: Invitrogen LanthaScreen TR-FRET LXR beta Coactivator Assay Kit (catalog no. PV4658); RARα: Invitrogen LanthaScreen TR-FRET RAR alpha Coactivator Assay Kit (catalog no. PV4409).
(50) Paulik, M. A.; Lenhard, J. M. Thiazolidinediones inhibit alkaline phosphatase activity while increasing expression of uncoupling protein, deiodinase, and increasing mitochondrial mass in C3H10T1/2 cells. *Cell Tissue Res.* **1997**, *290*, 79–87.
(51) Weihua, Z.; Lathe, R.; Warner, M.; Gustafsson, J. A. An endocrine pathway in the prostate, ERbeta, AR, 5alpha-androstane-3beta,17beta-diol, and CYP7B1, regulates prostate growth. *Proc. Natl. Acad. Sci. U.S.A.* **2002**, *99*, 13589–13594.
(52) We have maintained the original protein sequence numbering convention of Swiss-Prot P11474 (sequence version 2) in order to facilitate comparison with previous structures.[32,33] Accordingly, in our structure, electron density is defined from part of the polyhistidine tag and PreScission cleavage sequences [HHLEVLFQG-ERRα-LBD (289−519)]; no electron density for 519 is observed.
(53) Nuss, J. M.; Wagman, A. S. Recent advances in therapeutic approaches to type 2 diabetes. *Annu. Rep. Med. Chem.* **2000**, *35*, 211–220.
(54) Nolte, R. T.; Wisely, G. B.; Westin, S.; Cobb, J. E.; Lambert, M. H.; Kurokawa, R.; Rosenfeld, M. G.; Willson, T. M.; Glass, C. K.; Milburn, M. V. Ligand binding and co-activator assembly of the peroxisome proliferator-activated receptor-γ. *Nature* **1998**, *395*, 137–143.
(55) West, D. B.; Boozer, C. N.; Moody, D. L.; Atkinson, R. L. Dietary obesity in nine inbred strains of mice. *Am. J. Physiol.* **1992**, *262*, R1025–R1032.
(56) Surwit, R. S.; Kuhn, C. M.; Cochrane, C.; McCubbin, J. A.; Feinglos, M. N. Diet-induced type II diabetes in C57BL/6J mice. *Diabetes* **1988**, *37*, 1163–1167.
(57) Ahren, B.; Simonsson, E.; Scheurink, A. J. W.; Mulder, H.; Myrsen, U.; Sundler, F. Dissociated insulinotropic sensitivity to glucose and carbachol in high-fat diet-induced insulin resistance in C57BL/6J mice. *Metabolism* **1997**, *46*, 97–106.
(58) Baell, J. B.; Holloway, G. A. New substructure filters for removal of pan assay interference compounds (PAINS) from screening libraries and for their exclusion in bioassays. *J. Med. Chem.* **2010**, *53*, 2719–2740.
(59) Daniels, T.; Wang, X.; Shaughnessy, S.; Calvo, J.; Lindsley, L.; Li, X.; Stevenson, S.; Rangwala, S. The Effects of High Fat Diet and Exercise on the Metabolic Phenotype of ERRα Deficient Mice. Presented at the NAASO Obesity Society Annual Meeting, Boston, MA, October 20−24, **2006**.

(60) Villena, J. A.; Kralli, A. ERRalpha: a metabolic function for the oldest orphan. *Trends Endocrinol. Metab.* **2008**, *19*, 269–276.
(61) Dufour, C. R.; Wilson, B. J.; Huss, J. M.; Kelly, D. P.; Alaynick, W. A.; Downes, M.; Evans, R. M.; Blanchette, M.; Giguère, V. Genome-wide orchestration of cardiac functions by the orphan nuclear receptors ERRalpha and gamma. *Cell Metab.* **2007**, *5*, 345–356.
(62) Brunger, A. T.; Adams, P. D.; Clore, G. M.; DeLano, W. L.; Gros, P.; Grosse-Kunstleve, R. W.; Jiang, J. S.; Kuszewski, J.; Nilges, M.; Pannu, N. S.; Read, R. J.; Rice, L. M.; Simonson, T.; Warren, G. L. Crystallography & NMR system: a new software suite for macromolecular structure determination. *Acta Crystallogr., Sect. D: Biol. Crystallogr.* **1998**, *54*, 905–921.
(63) Jones, T. A.; Zou, J. Y.; Cowan, S. W.; Kjeldgaard, M. Improved methods for building protein models in electron density maps and the location of errors in these models. *Acta Crystallogr. A* **1991**, *47*, 110–119.
(64) Emsley, P.; Cowtan, K. Coot: model-building tools for molecular graphics. *Acta Crystallogr., Sect. D: Biol. Crystallogr.* **2004**, *60*, 2126–2132.
(65) Adams, P. D.; Grosse-Kunstleve, R. W.; Hung, L.-W.; Ioerger, T. R.; McCoy, A. J.; Moriarty, N. W.; Read, R. J.; Sacchettini, J. C.; Sauter, N. K.; Terwilliger, T. C. PHENIX: building new software for automated crystallographic structure determination. *Acta Crystallogr., Sect. D: Biol. Crystallogr.* **2002**, *58*, 1948–1954.